Multi-channel Blind System Identification for Central Hemodynamic Monitoring

by

Yi Zhang

Bachelor of Engineering in Mechanical Engineering
Tsinghua University, 1995

Master of Science in Mechanical Engineering
Massachusetts Institute of Technology, 2000

Master of Science in Electrical Engineering and Computer Science
Massachusetts Institute of Technology, 2000

Submitted to the Department of Mechanical Engineering
in Partial Fulfillment of the Requirements for the Degree of

Doctor of Philosophy

at the

Massachusetts Institute of Technology
September 2002

Signature of Author _____
Department of Mechanical Engineering
August 9. 2002

Certified by _____
H. Harry Asada
Ford Professor of Mechanical Engineering
Thesis Supervisor

Accepted by _____
Ain A. Sonin
Chairman, Department Committee on Graduate Students

Multi-channel Blind System Identification for Central Hemodynamic Monitoring

by

Yi Zhang

Submitted to the Department of Mechanical Engineering on August 9, 2002
in Partial Fulfillment of the Requirements for the Degree of
Doctor of Philosophy

ABSTRACT

Multi-channel Blind System Identification (MBSI) is a technique for estimating both an unknown input and unknown channel dynamics from simultaneous output measurements at different channels through which the input signal propagates. It is a powerful tool particularly for the identification and estimation of dynamical systems in which a sensor, for measuring the input, is difficult to place. All of the existing MBSI algorithms, however, are not applicable to multi-channel systems sharing common dynamics among the channels, since these algorithms, by nature, exploit "differences" among the multiple channel dynamics. This requirement renders the MBSI algorithms useless in systems that have both a lumped-parameter nature and a distributed nature; all channels in a system of this type share poles dictated by the lumped-parameter dynamics.

To overcome this difficulty, this thesis investigates a new approach, Intermediate Input Identification (IIID). This thesis proves that the distinct dynamics in each channel can be identified up to a scalar factor even when common dynamics are present. Based on this discovery, the MBSI problem is reformulated and an intermediate input is introduced, which integrates the original system input and the common dynamics shared by all the channels. The two-step IIID approach is developed to solve the problem: first, the distinct dynamics are identified from the outputs; second, the common dynamics are identified from the intermediate input by exploiting the zero-input response of the system. The identifiability conditions are thoroughly investigated. The sufficient and necessary conditions and the relationship between the linear-complexity condition of the original input and that of the intermediate input are derived in this thesis.

This thesis also develops a central hemodynamic monitoring scheme based on IIID. The similarities between the structure of a digital wireless communication system and that of the cardiovascular system are explained. The input, the common dynamics and the distinct dynamics in the cardiovascular multi-channel system are derived based on the determinants of arterial blood pressure. Analysis of the data from a cardiovascular simulator and animal experiments verify the validity of this scheme. The positive results demonstrate that the IIID approach could open up the possibility for noninvasive central hemodynamic monitoring, which could significantly reduce the risks to which patients are exposed.

Thesis Committee:
Dr. H. Harry Asada, Chair
Ford Professor of Mechanical Engineering
Dr. George Barbastathis
Esther and Harold E. Edgerton Assistant Professor of Mechanical Engineering
Dr. Roger G. Mark
Distinguished Professor of Health Sciences and Technology, Professor of Electrical Engineering

Acknowledgements

This thesis would not have been possible without the following people.

I would like to start off by thanking my thesis advisor, Professor Harry Asada, for giving me the opportunity to work in his group during my graduate study. I am thankful for the unique learning environment in this group. I am especially grateful to his concern about my professional development. I could not have achieved what I have done in the past five years without his support and encouragement.

I offer my sincere gratitude to the other members of my thesis committee, Professor George Barbastathis and Professor Roger Mark. Their participation, comments, and suggestions greatly enhanced this thesis. Particularly, I thank Dr. Mark for his great help on the animal experiments.

I am grateful to Dr. Andrew Reisner and Dr. Ramakrishna Mukkamala, for the constructive discussions we had and for the insights they provided to this work from a medical and an engineering perspective. I am especially indebted to them for their generous help and support for the animal study.

I would like to express my appreciation to the following individuals for their special contributions to this thesis: to Professor Roger Kamm for making the cardiovascular simulator available to me, to Xinshu (Grace) Xiao and Dr. Mohammad Kaazempur-Mofrad for helping me understand the simulator, to Thomas Heldt for providing the rabbit data, to Dr. Horacia Hojman for the animal study, to Professor Richard Cohen, Ping (Cindy) Liu and Phillip Shaltis for the constructive discussions and insightful comments, to Dr. Steve Mascaro, Devin McCombie and Phillip Shaltis for proof-reading my thesis, to Melissa Barbagelata for helping edit the thesis.

I would like to thank all the members of Professor Asada's group, both past and present. They have made my life at MIT much easier than what it could have been. I am also thankful to those individuals who have given me their friendship during my study at MIT. Thanks for making my life colorful.

Most of all, I would like to thank my husband and best friend, Haiyang Liu, who has been a companion, critic, and colleague, from whom I have learnt more and found more inspiration than any degree could possibly present, and for whom I have boundless love and respect.

My parents, Guohua and Xinhua, and my sister, Nan, deserve special thanks for their everlasting love through the years.

I dedicate this thesis to my grandparents.

Table of Contents

List of Figures

Chapter 1 Introduction

Central aortic pressure and flow tracings convey important information about the cardiovascular status and the cardiac performance. Traditionally, aortic flow and pressure recordings have required invasive catheterization, which may lead to bleeding, infection and sometimes thrombo-embolic complications [1]. The challenge in central hemodynamic monitoring is that the central flow and pressure, the input to the arterial system, are not easily measurable. The unavailability of the input is also a common issue in many biomedical and biological systems.

1.1 Inverse Transfer Function

Recent studies [2] suggest that the central pressure can be estimated by mathematically transforming peripheral pressure that is measured non-invasively. This method is referred as the inverse transfer function method in this thesis. The objective of extracting central information from peripheral noninvasive measurements is achieved by deriving a general model from the central to the peripheral pressure. First, invasive central measurements and noninvasive peripheral measurements are taken for a group of subjects. Second, the transfer function for each subject in the group is identified. Finally, the average of all the transfer functions is used as the general model for predictions on other subjects.

The inverse transfer function method, however, has two major disadvantages. First, an invasive central measurement is still necessary to identify the individual transfer functions from the central pressure (system input) to the peripheral pressure (system output). Second, an averaged transfer function has to be used to predict the input from the output on other subjects. Since the cardiovascular system is highly time varying and subject dependent, this general model has limited applicability.

1.2 Blind System Identification

In this thesis, a new approach to monitor central aortic flow using the multi-channel blind system identification (MBSI) technique is presented. MBSI is the technique that allows the estimation of both unknown input and unknown channel dynamics from only channel outputs. I was inspired by

the application of MBSI to wireless communication systems [3], where a broadcast signal is transmitted through different paths and received simultaneously by multiple receivers, as illustrated in Figure 1. Both the unknown channel dynamics and the unknown source signal are reconstructed by exploring the correlation among the signals received at different locations.

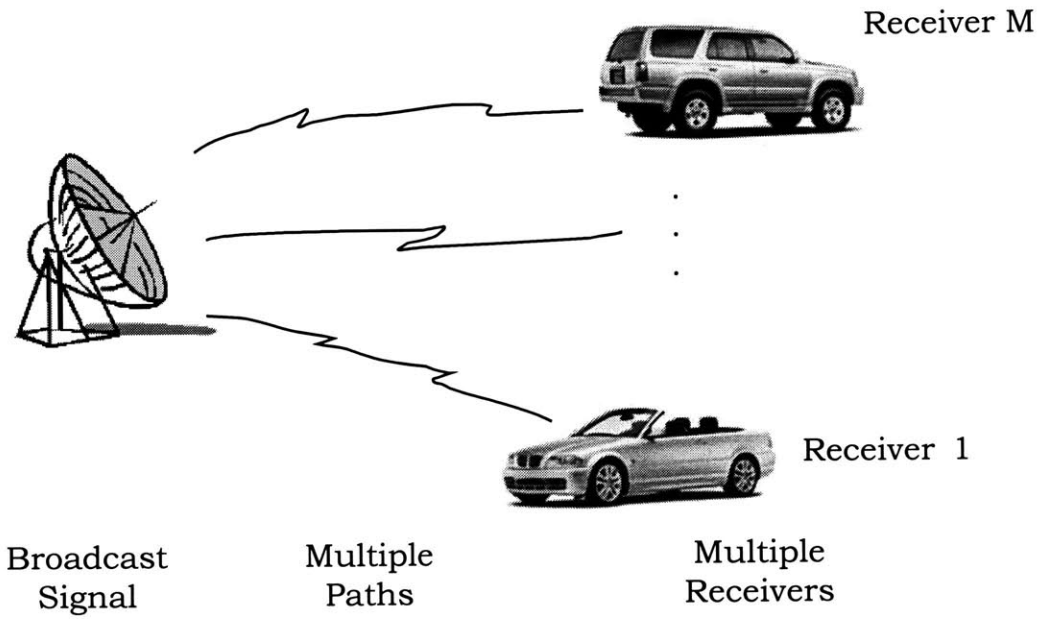

Figure 1. Digital Wireless Communication System

It is noticed that the arterial system has a structure topologically similar to the wireless communication system. As illustrated in Figure 2, the three major branches of the aorta, the brachiocephalic trunk, the left common carotid artery and the left subclavian artery, disperse into different parts of the body. In general, systemic circulation is modeled as a multi-channel system as follows: the left ventricle is modeled as a flow source that is characterized by the cardiac output, the common input to the system; different arterial branches are modeled as the different channels of the system; noninvasive sensors, located at different branches of the systemic circulatory system, are the outputs which are driven by the common input. Figure 3 depicts the schematic of such an arterial multi-channel system. Central hemodynamics, i.e., the source, are transmitted through different arterial paths and observed at multiple systemic locations, such as the carotid, the subclavian, the femoral, etc. If multiple sensors are placed at different systemic locations, the MBSI technique can be applied to estimate the arterial channel dynamics and the aortic flow. This new technique could open up the possibility of noninvasive central hemodynamic monitoring, which could significantly reduce the risks exposed to patients.

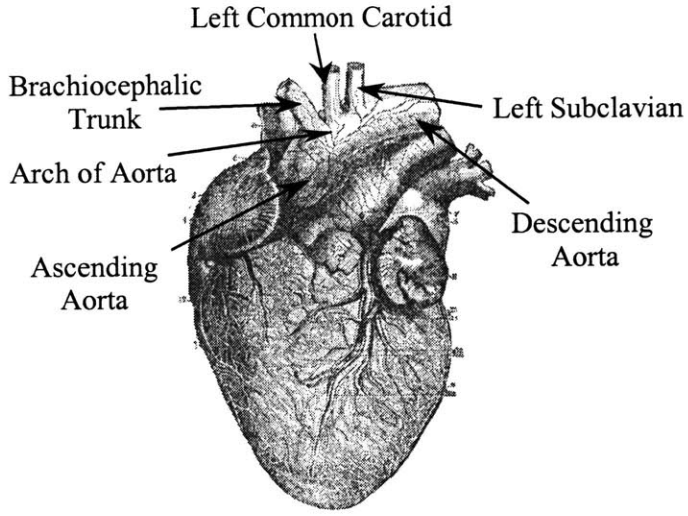

Figure 2. Anatomy of the Systemic Circulatory System

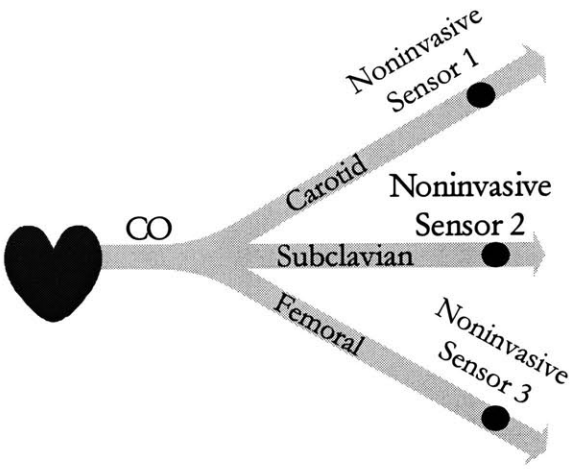

Figure 3. Schematic of an Arterial Multi-channel System

1.3 Thesis Scope and Organization

To apply MBSI theory, however, several conditions must be met. These conditions are not directly satisfied when applying MBSI to central hemodynamic monitoring. This thesis presents an effective solution to this problem. The rest of the thesis is organized in the following way:

Chapter 2 will review the existing MBSI algorithms, discuss the identifiable and non-identifiable systems and raise the issue of common dynamics. Chapter 3 will introduce the new formulation of the MBSI problem with common dynamics, develop the theorems for the identification of the distinct dynamics and the common dynamics, and propose the intermediate

input identification approach to solve the MBSI problem with common dynamics. Numerical examples will be provided to illustrate the theorems of distinct dynamics identification. Chapter 4 will focus on the application of the intermediate input identification approach to central aortic flow monitoring. The concept of modeling the arterial hemodynamics as a multi-channel system will be described first. The identification conditions of the arterial system will be analyzed. Numerical simulations results using a cardiovascular simulator will be presented. Chapter 5 will provide experimental results from animal studies. Chapter 6 will summarize the contributions of this thesis and propose the directions for future research.

Chapter 2 Multi-channel Blind System Identification

MBSI is the technique that allows the estimation of both an unknown input and unknown channel dynamics from multiple channel outputs. Figure 4 shows the schematic of a multi-channel system, the key feature of which is that all the channels are driven by the same input. Therefore the inherent correlation among the outputs can be explored to solve the problem.

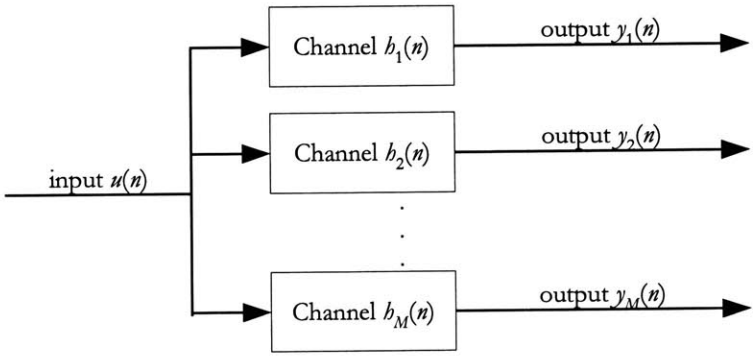

Figure 4. Schematic of a Multi-channel System

This chapter will start with a review of existing MBSI algorithms, which focuses on deterministic approaches. The cross relation among the outputs and its different forms in different types of systems, i.e.: all-zero systems, all-pole systems and pole-zero systems, will be introduced first. The least-squares solution to the MBSI problem exploiting this relation will then be derived. The formulations for different types of systems will then be generalized into one form, which will be referred to in the rest of the thesis. Next, the identifiability conditions, namely the sufficient-output condition, the input-linear-complexity condition and the distinct-channel condition, will be discussed, both qualitatively and quantitatively. In particular, the sufficient and necessary requirements on the input linear complexity will be derived for all-pole systems and pole-zero systems. Finally, the problem of the existing algorithms in dealing with multi-channel systems when common dynamics are present will be addressed.

2.1 Review of Existing MBSI Algorithms

There are two types of MBSI algorithms. Stochastic algorithms exploit the statistical information of the input, such as probability density function [3], cyclostationarity [4][5], etc. However, such a statistical model may not always be available, or there may not be enough data samples to find a reasonably accurate estimate. On the other hand, deterministic algorithms, which will be the focus of this section, do not assume any statistical property of the input, but rather treat the input as a deterministic signal. They explore the cross relation among the outputs that is inherent in multiple-output systems. The content of this section is a summary of [3][6][7][8][9][10].

2.1.1 Problem Formulation

The multiple channels shown in Figure 4 are driven by the same unknown input, denoted by $u(n)$, and yield different outputs, denoted by $y_1(n)$, $y_2(n)$, ... , $y_M(n)$, where M denotes the number of channels. Assuming that the channels are linear and time-invariant (LTI) and their impulse responses are denoted by $h_1(n)$, $h_2(n)$, ... , $h_M(n)$, the system is described in time domain by the following model:

$$\begin{cases} y_1(n) = h_1(n) * u(n) \\ y_2(n) = h_2(n) * u(n) \\ \quad \vdots \\ y_M(n) = h_M(n) * u(n) \end{cases} \tag{1}$$

where * denotes the linear convolution. The MBSI problem is stated as follows: Given the observations of the channels' outputs $y_1(n)$, $y_2(n)$, ... , $y_M(n)$, determine the channels' dynamics $h_1(n)$, $h_2(n)$, ... , $h_M(n)$ and ultimately recover the input signal $u(n)$.

Let $U(z^{-1})$ and $Y_i(z^{-1})$, $i = 1, 2, \ldots, M$, denote the z-transform of the corresponding signal $u(n)$ and $y_i(n)$, $i = 1, 2, \ldots, M$, respectively. The system model can then be written in frequency domain as:

$$\begin{cases} Y_1(z^{-1}) = H_1(z^{-1}) * U(z^{-1}) \\ Y_2(z^{-1}) = H_2(z^{-1}) * U(z^{-1}) \\ \quad \vdots \\ Y_M(z^{-1}) = H_M(z^{-1}) * U(z^{-1}) \end{cases} \tag{2}$$

where $H_1(z^{-1})$, $H_2(z^{-1})$, ... , $H_M(z^{-1})$ denote the transfer function of each channel. Let $N_i(z^{-1})$ and $D_i(z^{-1})$, $i = 1, 2, \ldots, M$, denote the numerator and the denominator of each transfer function respectively. The transfer functions then have the following general form:

$$H_i(z^{-1}) = \frac{Y_i(z^{-1})}{U(z^{-1})} = \frac{N_i(z^{-1})}{D_i(z^{-1})} = \frac{b_{i,0} + b_{i,1}z^{-1} + ... + b_{i,m_i}z^{-m_i}}{1 + a_{i,1}z^{-1} + ... + a_{i,n_i}z^{-n_i}}, i = 1, 2, ..., M \quad (3)$$

where n_i and m_i are the number of poles and zeros in channel i respectively; $a_{i,1}, \ldots, a_{i,n_i}, i = 1, 2, ..., M$, are the coefficients of the polynomial $D_i(z^{-1})$, $i = 1, 2, \ldots, M$; $b_{i,0}, \ldots, b_{i,m_i}, i = 1, 2, ..., M$, are the coefficients of the polynomial $N_i(z^{-1})$, $i = 1, 2, \ldots, M$.

2.1.2 Cross Relation Between Two Channel Outputs

Consider any two noise-free outputs of the multi-channel system, $y_i(n)$ and $y_j(n)$:

$$\begin{aligned} y_i(n) &= h_i(n) * u(n) \\ y_j(n) &= h_j(n) * u(n) \end{aligned} \quad (4)$$

The two outputs have the following cross relation since they are driven by the same input:

$$\begin{aligned} h_i(n) * y_j(n) &= h_i(n) * [h_j(n) * u(n)] \\ &= h_j(n) * [h_i(n) * u(n)] \\ &= h_j(n) * y_i(n) \end{aligned} \quad (5)$$

This relation can be written in frequency domain as:

$$\begin{aligned} H_i(z^{-1}) * Y_j(z^{-1}) &= H_i(z^{-1}) * [H_j(z^{-1}) * U(z^{-1})] \\ &= H_j(z^{-1}) * [H_i(z^{-1}) * U(z^{-1})] \\ &= H_j(z^{-1}) * Y_i(z^{-1}) \end{aligned} \quad (6)$$

The cross relation in eq. (6) takes different forms for different types of systems.

a) All-zero Systems

When all the poles of the channels are located at the origin, i.e.: $D_i(z^{-1}) = 1$ for $i = 1, 2, \ldots, M$, the channel dynamics are described by a moving average (MA) model:

$$H_i(z^{-1}) = N_i(z^{-1}) = b_{i,0} + b_{i,1}z^{-1} + \ldots + b_{i,m_i}z^{-m_i}, i = 1, 2, ..., M \quad (7)$$

The cross relation between the outputs of the all-zero system is:

$$N_i(z^{-1})Y_j(z^{-1}) = N_j(z^{-1})Y_i(z^{-1}) \quad (8)$$

b) All-pole Systems

When all the zeros of the channels are located at the origin, i.e.: $N_i(z^{-1}) = 1$ for $i = 1, 2, \ldots, M$, the channel dynamics are described by an auto-regressive (AR) model:

$$H_i(z^{-1}) = \frac{1}{D_i(z^{-1})} = \frac{1}{a_{i,0} + a_{i,1}z^{-1} + \ldots + a_{i,n_i}z^{-n_i}}, i = 1, 2, \ldots, M \tag{9}$$

The cross relation between the outputs of the all-pole system is:

$$Y_j(z^{-1})D_j(z^{-1}) = Y_i(z^{-1})D_i(z^{-1}) \tag{10}$$

c) Pole-zero Systems

When both poles and zeros are present, the channel dynamics are described by an auto-regressive moving average (ARMA) model:

$$H_i(z^{-1}) = \frac{N_i(z^{-1})}{D_i(z^{-1})} = \frac{b_{i,0} + b_{i,1}z^{-1} + \ldots + b_{i,m_i}z^{-m_i}}{a_{i,0} + a_{i,1}z^{-1} + \ldots + a_{i,n_i}z^{-n_i}}, i = 1, 2, \ldots, M \tag{11}$$

The cross relation between the output of the pole-zero system is:

$$Y_j(z^{-1})[D_j(z^{-1})N_i(z^{-1})] = Y_i(z^{-1})[D_i(z^{-1})N_j(z^{-1})] \tag{12}$$

2.1.3 Identification Exploiting the Cross Relation

The above cross relations show that each pair of outputs in the multi-channel system is related by their channels' responses. Clearly, when there are adequate data samples of the outputs, the MBSI problem is cast into an over-determined least-squares problem. Under certain conditions that will be elaborated in section 2.2, the channel dynamics can be determined uniquely up to a scalar factor. In the following formulation, N denotes the number of input samples; L denotes the maximum order of all the channels, whose meaning in the all-zero, the all-pole and the pole-zero systems will be given in each of the following sections; the input sequence is denoted by $u(n)$, $n = 1, \ldots, N$; the output sequences are denoted by $y_i(n)$, $i = 1, \ldots, M$, $n = L, \ldots, N$.

a) All-zero Systems

An all-zero channel has a finite impulse response (FIR). In fact, eq. (7) suggests that:

$$h_i(n) = \begin{cases} b_{i,n-1}, n = 1, 2, ..., m_i + 1 \\ 0, \quad \text{otherwise} \end{cases}, i = 1, 2, ..., M \tag{13}$$

The channel order is determined by the length of the impulse response, i.e.: m_i+1. L is defined as the maximum length of the impulse response of all the channels, i.e.: $max(m_i+1, i = 1, 2, ..., M)$. Eq. (8) is rearranged as a set of linear equations of $h_i(n)$ and $h_j(n)$:

$$[\mathbf{Y}_i, \ -\mathbf{Y}_j] \begin{bmatrix} \mathbf{h}_j \\ \mathbf{h}_i \end{bmatrix} = 0 \tag{14}$$

where $\mathbf{h}_k \equiv [h_k(L), \ \cdots, \ h_k(1)]^T, k = i, j$, and

$$\mathbf{Y}_k \equiv \begin{bmatrix} y_k(L) & y_k(L+1) & \cdots & y_k(2L-1) \\ y_k(L+1) & y_k(L+2) & \cdots & y_k(2L) \\ \vdots & \vdots & \ddots & \vdots \\ y_k(N-L+1) & y_k(N-L+2) & \cdots & y_k(N) \end{bmatrix}, k = i, j \tag{15}$$

For each pair of outputs in the multi-channel system, we can write a set of linear equations as eq. (14). Combining all of the permutations among M channels, we can write a larger set of linear equations in terms of $\mathbf{h}_1, \mathbf{h}_2, ..., \mathbf{h}_M$:

$$\mathbf{Y} \cdot \mathbf{h} = 0 \tag{16}$$

where $\mathbf{h} \equiv [\mathbf{h}_1{}^T, \ \cdots, \ \mathbf{h}_M{}^T]^T$ and

$$\mathbf{Y} \equiv \begin{bmatrix} \mathbf{Y}_2 & -\mathbf{Y}_1 & 0 & 0 & \cdots & 0 \\ \mathbf{Y}_3 & 0 & -\mathbf{Y}_1 & 0 & \cdots & 0 \\ 0 & \vdots & \vdots & \vdots & \ddots & 0 \\ \mathbf{Y}_M & 0 & 0 & \cdots & 0 & -\mathbf{Y}_1 \\ 0 & \mathbf{Y}_3 & -\mathbf{Y}_2 & 0 & \cdots & 0 \\ \vdots & \vdots & \vdots & \vdots & \ddots & \vdots \\ 0 & \mathbf{Y}_M & 0 & \cdots & 0 & -\mathbf{Y}_2 \\ \vdots & \vdots & \vdots & \vdots & \vdots & \vdots \\ 0 & \cdots & \cdots & 0 & \mathbf{Y}_M & -\mathbf{Y}_{M-1} \end{bmatrix} \tag{17}$$

$\mathbf{h}$ can be solved by the least-squares estimate within a scalar factor.

b) All-pole Systems

An all-pole channel has an infinite impulse response (IIR). The channel order in this case is determined by the order of the polynomial $D_i(z^{-1})$, i.e.: n_i. L is defined as the maximum number of poles of all the channel, i.e.: $max(n_i, i = 1, 2, \ldots, M)$. Eq. (10) is rearranged as a set of linear equations:

$$[\mathbf{Y}_i, \ -\mathbf{Y}_j]\begin{bmatrix}\mathbf{D}_i \\ \mathbf{D}_j\end{bmatrix} = 0 \tag{18}$$

where $\mathbf{D}_k \equiv [a_{k,n_k}, \ \cdots, \ a_{k,1}]^T, k = i, j$, and $\mathbf{Y}_k, k = i, j$ is as defined in eq. (15).

Similarly, for multiple channels, combining all of the permutations among M channels results in a set of linear equations in terms of $\mathbf{D}_1, \mathbf{D}_2, \ldots, \mathbf{D}_M$:

$$\mathbf{Y} \cdot \mathbf{D} = 0 \tag{19}$$

where $\mathbf{D} \equiv \left[\mathbf{D}_1{}^T, \ \cdots, \ \mathbf{D}_M{}^T\right]^T$ and

$$\mathbf{Y} \equiv \begin{bmatrix}
\mathbf{Y}_1 & -\mathbf{Y}_2 & 0 & 0 & \cdots & 0 \\
\mathbf{Y}_1 & 0 & -\mathbf{Y}_3 & 0 & \cdots & 0 \\
0 & \vdots & \vdots & \vdots & \ddots & 0 \\
\mathbf{Y}_1 & 0 & 0 & \cdots & 0 & -\mathbf{Y}_M \\
0 & \mathbf{Y}_2 & -\mathbf{Y}_3 & 0 & \cdots & 0 \\
\vdots & \vdots & \vdots & \vdots & \ddots & \vdots \\
0 & \mathbf{Y}_2 & 0 & \cdots & 0 & -\mathbf{Y}_M \\
\vdots & \vdots & \vdots & \vdots & \vdots & \vdots \\
0 & \cdots & \cdots & 0 & \mathbf{Y}_{M-1} & -\mathbf{Y}_M
\end{bmatrix} \tag{20}$$

Notice the difference in matrix $\mathbf{Y}$ for the all-zero system (eq. (17)) and the all-pole system (eq. (20)).

c) Pole-zero System

A pole-zero channel also has an IIR. The channel order in this case is determined by the number of coefficients in the polynomial $D_i(z^{-1})N_j(z^{-1})$, i.e.: the number of poles in channel i and the number of zeros in channel j plus one. L is defined as $max(n_i + m_j + 1, n_j + m_i + 1, i \neq j)$.

In this case, at least three channels are necessary to distinguish poles and zeros of each channel. First, eq. (12) is rearranged as follows to solve for the roots of the polynomials $D_i(z^{-1})N_j(z^{-1})(i, j = 1,...,M, i \neq j)$:

$$[\mathbf{Y}_i, \ -\mathbf{Y}_j]\begin{bmatrix}\mathbf{D}_i\mathbf{N}_j \\ \mathbf{D}_j\mathbf{N}_i\end{bmatrix} = 0 \tag{21}$$

where $\mathbf{D}_i\mathbf{N}_j$ and $\mathbf{D}_j\mathbf{N}_i$ are the vectors whose elements are the coefficients of the polynomials $D_i(z^{-1})N_j(z^{-1})$ and $D_j(z^{-1})N_i(z^{-1})$. Then, consider the set of polynomials $D_i(z^{-1})N_j(z^{-1})$, $j = 1,...,M, i \neq j$, which may be considered as the outputs of a (M-1)-channel FIR system driven by $D_i(z^{-1})$ and having channel transfer function $N_j(z^{-1})$, $j = 1,...,M, i \neq j$. The schematic of this all-zero system is illustrated in Figure 5. The zero locations of each channel can then be solved by formulating another MBSI problem for this all-zero system. The pole locations can be solved in a similar manner by formulating an MBSI problem for the all-zero system shown in Figure 6.

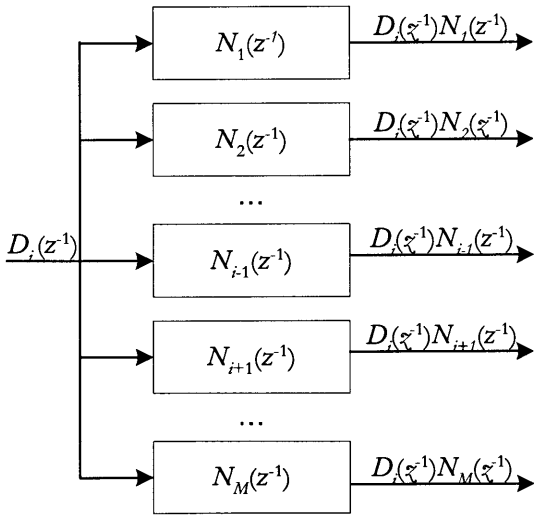

Figure 5. An All-zero System Formulated to Solve the Zero Locations of a Pole-Zero System

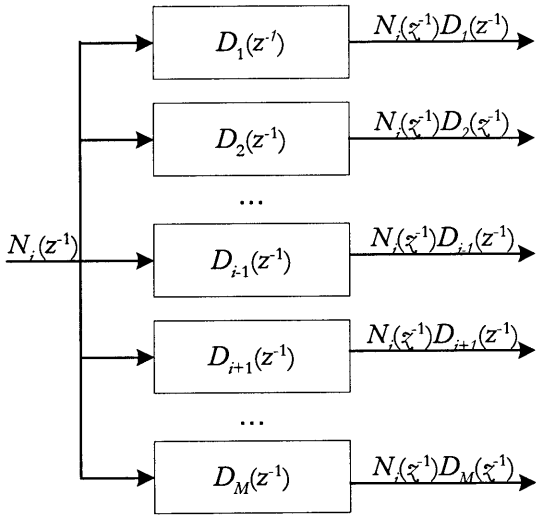

Figure 6. An All-zero System Formulated to Solve the Pole Locations of a Pole-Zero System

This procedure is illustrated by the following example. Given a three-channel system whose channel dynamics are described by the following transfer functions:

$$\frac{Y_i(z^{-1})}{U(z^{-1})} = \frac{N_i(z^{-1})}{D_i(z^{-1})}, i = 1,2,3 \tag{22}$$

All the polynomials in eq. (22) are co-prime. A two-step procedure is needed to identify the distinct dynamics in the system. $\Omega\{\bullet\}$ denotes the roots of a polynomial $\bullet$.

First step: three two-channel BSI

$$\begin{matrix} y_1 \\ y_2 \end{matrix} \Rightarrow \begin{matrix} \Omega\{D_1(z^{-1})N_2(z^{-1})\} \\ \Omega\{D_2(z^{-1})N_1(z^{-1})\} \end{matrix} \quad \begin{matrix} y_2 \\ y_3 \end{matrix} \Rightarrow \begin{matrix} \Omega\{D_2(z^{-1})N_3(z^{-1})\} \\ \Omega\{D_3(z^{-1})N_2(z^{-1})\} \end{matrix} \quad \begin{matrix} y_3 \\ y_1 \end{matrix} \Rightarrow \begin{matrix} \Omega\{D_3(z^{-1})N_1(z^{-1})\} \\ \Omega\{D_1(z^{-1})N_3(z^{-1})\} \end{matrix}$$

Second step: two two-channel BSI

$$\begin{matrix} \Omega\{D_1(z^{-1})N_2(z^{-1})\} \\ \Omega\{D_1(z^{-1})N_3(z^{-1})\} \end{matrix} \Rightarrow \begin{matrix} \Omega\{D_1(z^{-1})\} \\ \Omega\{N_2(z^{-1})\} \\ \Omega\{N_3(z^{-1})\} \end{matrix} \qquad \begin{matrix} \Omega\{D_2(z^{-1})N_1(z^{-1})\} \\ \Omega\{D_3(z^{-1})N_1(z^{-1})\} \end{matrix} \Rightarrow \begin{matrix} \Omega\{N_1(z^{-1})\} \\ \Omega\{D_2(z^{-1})\} \\ \Omega\{D_3(z^{-1})\} \end{matrix}$$

2.1.4 General Form of the MBSI Problem

In summary, the general form of the blind system identification problem for any pair of channels in the multi-channel system is:

$$[\mathbf{Y}_i, \quad -\mathbf{Y}_j] \begin{bmatrix} \mathbf{W}_i \\ \mathbf{W}_j \end{bmatrix} = 0 \tag{23}$$

where $\mathbf{Y}_i$ and $\mathbf{Y}_j$ have been defined in eq. (15) and $\mathbf{W}_i$ and $\mathbf{W}_j$ have different forms for different types of systems as defined in eq. (14), (18) and (21). This general form can be extended to the case of multi-channel systems using eq. (16), (17) or (19), (20).

For simplicity, in the rest of the thesis, all the algorithms will be derived for a two-channel system. The general form that will be used is:

$$\mathbf{Y}(L) \begin{bmatrix} \mathbf{W}_1(L) \\ \mathbf{W}_2(L) \end{bmatrix} \equiv [\mathbf{Y}_2(L), \quad -\mathbf{Y}_1(L)] \begin{bmatrix} \mathbf{W}_1(L) \\ \mathbf{W}_2(L) \end{bmatrix} = 0 \tag{24}$$

The parameter L indicates the maximum order of the two channels. The matrices in eq. (24) have the following dimensions:

$\mathbf{Y}(L) : (N - 2L + 2) \times 2L$
$\mathbf{Y}_1(L), \mathbf{Y}_2(L) : (N - 2L + 2) \times L$
$\mathbf{W}_1(L), \mathbf{W}_2(L) : L \times 1$

2.2 Identifiability Conditions

A direct observation from the general form, eq. (24), is that the channels' dynamics can be identified uniquely if and only if the dimension of the null space of the matrix $\mathbf{Y}(L)$ is 1, i.e.: one and only one column of the matrix $\mathbf{Y}(L)$ is a linear combination of the others. Qualitatively, given the channels' order L, the MBSI problem can be solved only when the following identifiability conditions [3] are met:

- The outputs must have enough samples.
- The input must be rich enough to excite all the modes in the system.
- All channels in the system must be distinct.

The first two conditions are general requirements for any system identification problem, e.g., the standard input-output identification problem [12], while the distinct-channel condition is unique to the MBSI problem. The quantitative descriptions of the three conditions are given in the following sections.

2.2.1 Sufficient-output Condition

The MBSI algorithms estimate the channel dynamics by solving a set of over-determined linear equations, thus requiring that the matrix $\mathbf{Y}(L)$ in eq. (24) have more rows than columns. As mentioned earlier, the matrix $\mathbf{Y}(L)$ has a dimension of $(N\text{-}2L+2)\times 2L$. Therefore the number of the output samples, $N\text{-}L+1$, has to satisfy

$$N - L + 1 \geq 3L - 1 \tag{25}$$

If the number of output samples is less than $3L\text{-}1$, then the linear equations in eq. (24) have more variables than equations. Thus the problem becomes an underdetermined problem and more than one solution exists.

2.2.2 Input-linear-complexity Condition

It is required that the input must be rich enough to excite all the modes in the channel dynamics. The richness of a finite sequence, $\{u(n), n = 1, \ldots, N\}$, is measured by the number of modes in the sequence, which is also referred to as the linear complexity. Quantitatively, the number of modes of the finite sequence $u(n)$, denoted by p, has the following property [6][11]:

Lemma 1: Given a finite sequence $u(n)$, $n = 1, 2, \ldots, N$. If there are p modes in the sequence $u(n)$, the p^{th}-order Hankel matrix $\mathbf{U}(p)$ defined in the following has full column rank:

$$\mathbf{U}(p) = \begin{bmatrix} u(1) & \cdots & u(p) \\ \vdots & \ddots & \vdots \\ u(N-p+1) & \cdots & u(N) \end{bmatrix} \tag{26}$$

The linear complexity of a finite sequence is analogous to the number of frequency components in an infinite data sequence, which is measured by the persistence of excitation of the signal:

Lemma 2 [12]: A quasi-stationary signal $u(n)$ is persistently exciting of order p if and only if the $p \times p$ Toeplitz matrix of the signal's auto-correlation, $\mathbf{R}(p)$ defined in the following, has full rank:

$$\mathbf{R}(p) = \begin{bmatrix} R_u(0) & R_u(1) & \cdots & R_u(p-1) \\ R_u(1) & R_u(0) & \cdots & R_u(p-2) \\ \vdots & \vdots & \ddots & \vdots \\ R_u(p-1) & R_u(p-2) & \cdots & R_u(0) \end{bmatrix} \tag{27}$$

where

$$R_u(i) = \frac{1}{N} \sum_{n=i}^{N} u(n-i)u(n), i \geq 0 \tag{28}$$

The sufficient and necessary conditions on the input linear complexity are given by the following theorem [6]:

Theorem 1: Assuming that there is no noise, when the channel order L is known, the sufficient and necessary conditions for the MBSI problem in eq. (24) are: *Sufficient Condition*: the MBSI problem has a unique solution if $p \geq 2L-1$; *Necessary Condition*: the MBSI problem does not have a unique solution if $p < L$.

In [6], Theorem 1 has been proved for the case of all-zero systems, which is summarized in Appendix A. However, it has not been proved for the case of all-pole systems and pole-zero systems because it is a general practice to assume FIR for digital communication systems. The proof for the case of all-pole systems and pole-zero systems is derived in this thesis.

Proof:

(*Necessity*) The proof of the necessary condition for the all-pole system and the pole-zero system is the same as for the all-zero system.

(*Sufficiency*) As mentioned earlier, if we can prove that rank{ $\mathbf{Y}(L)$ } =2L-1 when $p \geq 2L$-1, then eq. (24) has a unique solution. We will first prove rank{ $\mathbf{Y}(L)$ }$\leq$ 2L-1. Then prove that the rank of $\mathbf{Y}(L)$ cannot be less than 2L-1.

Each sample of the channel outputs, $y_i(k)$, is the convolution of the input, $u(n)$, with the impulse response of the corresponding channel, $h_i(n)$, i.e.:

$$y_i(k) = [u(k-L_h+1), \quad \cdots, \quad u(k)] \begin{bmatrix} h_i(L_h) \\ \vdots \\ h_i(1) \end{bmatrix}, i = 1, 2 \tag{29}$$

where L_h is the maximum length of the impulse responses in the two channels. Although namely an all-pole system or a pole-zero system has an infinitely long impulse response, it can always be approximated by a finite-length impulse response for a stable system, as long as L_h is sufficiently large. Therefore, it is reasonable to assume $L_h >> N$.

When L is known, W_1 and W_2 are vectors with dimension of $L \times 1$. The matrix $\mathbf{Y}(L)$ can be expressed as a multiplication of the input Hankel matrix $\mathbf{U}(L)$ and the impulse response matrix $\mathbf{H}(L)$:

$$\mathbf{Y}(L) = \mathbf{U}(L) \cdot \mathbf{H}(L) \tag{30}$$

where

$$\mathbf{U}(L) \equiv \begin{bmatrix} u(L-L_h+1) & \cdots & u(0) & u(1) & \cdots & u(2L-1) \\ \vdots & \ddots & \vdots & \vdots & \ddots & \vdots \\ u(N-L-L_h+2) & \cdots & u(N-2L+1) & u(N-2L+2) & \cdots & u(N) \end{bmatrix} : \{(N-2L+2) \times (L_h+L-1)\} \tag{31}$$

$$\mathbf{H}(L) \equiv [\mathbf{H}_2(L), \quad -\mathbf{H}_1(L)] : \{(L_h+L-1) \times 2L\} \tag{32}$$

$$\mathbf{H}_i(L) \equiv \begin{bmatrix} h_0(L_h) & & \\ \vdots & \ddots & \\ h_0(L_h - L + 1) & \cdots & h_0(L_h) \\ \vdots & \cdots & \vdots \\ h_0(1) & \cdots & h_0(L) \\ & \ddots & \vdots \\ & & h_0(1) \end{bmatrix} : \{(L_h + L - 1) \times L\}, i = 1, 2 \tag{33}$$

$p \geq 2L$-1 implies that $\mathbf{U}(L)$ has a row rank of at least $2L$-1. Also we know that rank$\{\mathbf{H}(L)\} = 2L$-1. Since rank$\{\mathbf{Y}(L)\} \leq$ rank$\{\mathbf{U}(L)\}$ and rank$\{\mathbf{Y}(L)\} \leq$ rank$\{\mathbf{H}(L)\}$, the rank of $\mathbf{Y}(L)$ is at most $2L$-1.

Now prove that the rank of $\mathbf{Y}(L)$ cannot be less than $2L$-1. Let u_i denote the i^{th} row of $\mathbf{U}(L)$, h_i denote the i^{th} column of $\mathbf{H}(L)$, y_i denote the i^{th} column of $\mathbf{Y}(L)$. They satisfy the following relation:

$$y_i = \begin{bmatrix} u_1 \\ \vdots \\ u_{N-L+1} \end{bmatrix} h_i, i = 1, 2, ..., 2L \tag{34}$$

Assume that rank$\{\mathbf{Y}(L)\} = 2L - 2$. Without loss of generality, assume that y_{2L-1} and y_{2L} are dependent, i.e.:

$$\begin{bmatrix} u_1 \\ \vdots \\ u_{N-L+1} \end{bmatrix} (h_{2L} - c_1 h_1 - ... - c_{2L-2} h_{2L-2}) = 0 \tag{35}$$

$$\begin{bmatrix} u_1 \\ \vdots \\ u_{N-L+1} \end{bmatrix} (h_{2L-1} - k_1 h_1 - ... - k_{2L-2} h_{2L-2}) = 0 \tag{36}$$

With $L_h > N > L$, the first $2L$-1 columns of $\mathbf{U}(L)$ are linearly independent, so the first $2L$-1 rows of $\mathbf{U}(L)$ are also linearly independent. Therefore, at least the first $2L$-1 elements in the column vector $h_{2L} - c_1 h_1 - ... - c_{2L-2} h_{2L-2}$ and $h_{2L} - k_1 h_1 - ... - k_{2L-2} h_{2L-2}$ are zero, which implies that the matrix that consists of first $2L$-1 rows of $\mathbf{H}(L)$ has a rank of $2L$-2. However, due to the special Hankel structure of the matrix $\mathbf{H}(L)$, the first $2L$-1 rows in $\mathbf{H}(L)$ make a diagonal matrix, so they are independent. Therefore the assumption that $\mathbf{Y}(L)$ has a rank of $2L$-2 is not correct. Thus,

$\mathbf{Y}(L)$ has a rank of $2L$-1; the dimension of the null space of the matrix $\mathbf{Y}(L)$ is 1. Therefore, the MBSI problem has a unique solution.

End of Proof.

2.2.3 Distinct-channel Condition

The distinct-channel condition requires that the poles and the zeros in one channel should be distinct from those in the other for a two-channel system to be identifiable. Otherwise, the algorithm cannot distinguish if the common dynamics come from the input or from the dynamics of the channels. For instance, if there is a common factor, $H_0(z^{-1})$, shared by the two channels, as in the two-channel system shown in Figure 7. The outputs of the system follow:

$$\begin{aligned} Y_1(z^{-1}) &= [H_0(z^{-1})H_1'(z^{-1})]U(z^{-1}) \\ Y_2(z^{-1}) &= [H_0(z^{-1})H_2'(z^{-1})]U(z^{-1}) \end{aligned} \tag{37}$$

Rearranging eq. (37), we have:

$$\begin{aligned} Y_1(z^{-1}) &= H_1'(z^{-1})[H_0(z^{-1})U(z^{-1})] \\ Y_2(z^{-1}) &= H_2'(z^{-1})[H_0(z^{-1})U(z^{-1})] \end{aligned} \tag{38}$$

which are the same as the outputs of the two-channel system shown in Figure 8. The two systems have exact the same outputs, but different channel dynamics and inputs. Given only the outputs, the MBSI algorithms summarized in section 2.1 cannot distinguish system 7 from system 8. Therefore, system 7 is treated as non-identifiable and system 8 is identifiable in the existing algorithms.

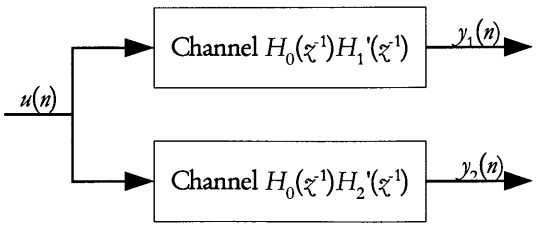

Figure 7. A Two-channel System with Common Dynamics

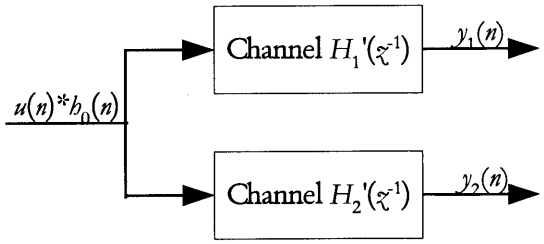

Figure 8. Another Two-channel System without Common Dynamics, but Having the Same Outputs as the One in Figure 7

2.3 Summary

From the above analysis, it is clear that existing MBSI algorithms can only deal with systems where no common dynamics are shared by all the channels. This is because the nature of the cross relation is to exploit the uniqueness of each channel. If there is a common factor in both channels, existing algorithms cannot distinguish between the input and the common dynamics.

This requirement limits the scope of the application of the existing algorithm. For instance, it renders the MBSI algorithms useless in systems that have both a lumped-parameter nature and a distributed nature, such as the cardiovascular system; all channels in a system of this type shares poles dictated by the lumped-parameter dynamics. To overcome this difficulty, this thesis investigates a new approach to simultaneously obtain the system dynamics (both the distinct part and common part of each channel dynamics) as well as the input from multiple outputs.

Chapter 3 Intermediate Input Identification Approach

MBSI is difficult when common dynamics are present in the multi-channel system because the modes in the input as well as the common dynamics are common for all the channels. Given only the outputs, the existing algorithms cannot distinguish between the input and the common dynamics. This is a problem that has not been tackled by previous research, although it is very common in practice, especially for the systems that have both a lumped-parameter nature and a distributed nature, such as the cardiovascular system.

An intuitive way to solve this problem is to remove the common dynamics before applying the cross relation algorithm [13]. If the common dynamics $H_0(z^{-1})$ in the system shown in Figure 7 can be identified from the outputs directly, then one can design an inverse filter to filter out the effect of the common dynamics. This approach improves the distinct-channel condition by removing the common dynamics in the channels. However, when the common dynamics are at low frequencies, a high-pass-filter will have to be applied to the outputs to remove the common mode, which tends to amplify the noises in the signals as well. Therefore, this approach has the disadvantage of being prone to noise when the common dynamics are at low frequency. Meanwhile, if there exist distinct dynamics in the same frequency range as the common dynamics, direct filtering will change the distinct dynamics in all the channels.

This chapter presents a different approach named the Intermediate Input IDentification (IIID) approach. First, the new formulation of the MBSI problem for systems with common dynamics will be introduced and the IIID approach will be proposed. Second, a series of lemmas and theorems will be derived to prove the existence and the uniqueness of the solution to the identification of the distinct dynamics. Additionally, theorems will be derived to explain what happens when the channel order is overestimated. Next, the method to identify the common dynamics by exploring the zero-input-dynamics will be developed. Finally, numerical examples will be given to illustrate the theorems.

3.1 Introduction

3.1.1 Systems with Common Dynamics

The two-channel system shown in Figure 7 will be studied throughout this chapter. In this system, $H_0(z^{-1})$ represents the transfer function of the common dynamics in both channels; $H_1'(z^{-1})$ and $H_2'(z^{-1})$ represent the transfer functions of the distinct dynamics in the two channels respectively; and $H_1(z^{-1})$ and $H_2(z^{-1})$ represent the overall transfer functions of the two channels respectively, i.e.:

$$H_i(z^{-1}) = H_i'(z^{-1})H_0(z^{-1}), i = 1, 2 \tag{39}$$

Let $N_i'(z^{-1})$ and $D_i'(z^{-1})$, i = 1, 2 denote the numerator and the denominator of $H_1'(z^{-1})$ and $H_2'(z^{-1})$ respectively. The transfer functions have the following general form:

$$H_i'(z^{-1}) = \frac{Y_i(z^{-1})}{V(z^{-1})} = \frac{N_i'(z^{-1})}{D_i'(z^{-1})} = \frac{b_{i,0}' + b_{i,1}'z^{-1} + \ldots + b_{i,m_i'}'z^{-m_i'}}{a_{i,0}' + a_{i,1}'z^{-1} + \ldots + a_{i,n_i'}'z^{-n_i'}}, i = 1, 2 \tag{40}$$

where n_i' and m_i' are the number of poles and zeros in the distinct dynamics of channel i respectively; $a_{i,0}', a_{i,1}', \ldots, a_{i,n_i'}', i = 1, 2$, are the coefficients of the polynomial $D_i'(z^{-1})$, i = 1, 2; $b_{i,0}', b_{i,1}', \ldots, b_{i,m_i'}', i = 1, 2$, are the coefficients of the polynomial N_i' (z^{-1}), i = 1, 2. Let $N_0(z^{-1})$ and $D_0(z^{-1})$ denote the numerator and the denominator of $H_0(z^{-1})$, the transfer function of the common dynamics is:

$$H_0(z^{-1}) = \frac{V(z^{-1})}{U(z^{-1})} = \frac{N_0(z^{-1})}{D_0(z^{-1})} = \frac{b_{0,0} + b_{0,1}z^{-1} + \ldots + b_{0,m_0}z^{-m_0}}{a_{0,0} + a_{0,1}z^{-1} + \ldots + a_{0,n_0}z^{-n_0}} \tag{41}$$

where n_0 and m_0 are the number of poles and zeros in the common dynamics of channel i respectively; $a_{0,0}, a_{0,1}, \ldots, a_{0,n_0}$, are the coefficients of the polynomial $D_0(z^{-1})$, $b_{0,0}, b_{0,1}, \ldots, b_{0,m_0}$ are the coefficients of the polynomial $N_0(z^{-1})$.

3.1.2 New MBSI Problem Formulation for Systems with Common Dynamics

It is known that the outputs of a multi-channel system must be correlated in some way since both channels are driven by the same input. This is also true for systems with common dynamics. In the thesis investigation, it is found that when the cross relation algorithm is applied to the outputs of a

system with common dynamics, under certain conditions, the result reveals the channel dynamics that are distinct to each channel, e.g., $H_1'(z^{-1})$ and $H_2'(z^{-1})$. In other words, the distinct dynamics can be uniquely identified even when common dynamics are present. This discovery led to the introduction of a new variable – the intermediate input and the new formulation of the MBSI problem for systems with common dynamics.

Revisit the two-channel system shown in Figure 7. If the system is linear, the two-channel system could be rearranged as the one in Figure 9. This is attributed to the interchangeability of linear dynamics. The core idea of this new formulation is to treat the common dynamics as part of the input. The intermediate variable $v(n)$, whose z-transform is denoted by $V(z^{-1})$, is treated as the input to the new multi-channel system. As will be proven in section 3.2, the distinct dynamics in the original system can be identified by solving the general form eq. (24). The dynamic equations of the new multi-channel system in the frequency domain are:

$$\begin{aligned} Y_i(z^{-1}) &= H_i(z^{-1})U(z^{-1}) \\ &= H_i'(z^{-1})H_0(z^{-1})]U(z^{-1}) \\ &= H_i'(z^{-1})[H_0(z^{-1})U(z^{-1})] \\ &= H_i'(z^{-1})V(z^{-1}), i = 1,2 \end{aligned} \tag{42}$$

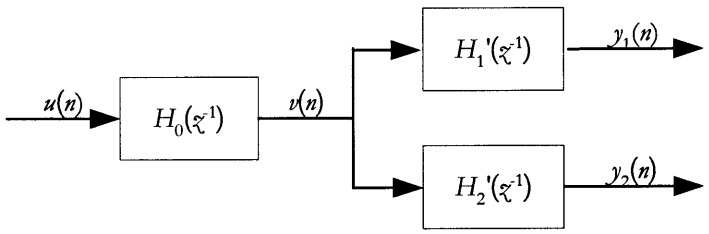

Figure 9. New MBSI Problem Formulation When Common Dynamics are Present

3.2 Distinct Dynamics Identification

The formulation and the solution of the distinct dynamics identification problem will be given in this section. The uniqueness of the solution will be proved for two scenarios: 1) when the exact order of the distinct dynamics is known; 2) when the exact order of the distinct dynamics is unknown, but an upper limit on the order is given. The sufficient and necessary conditions will be derived in terms of the identifiability conditions. The sufficient-output condition is the same as

before: output must be sufficiently long such that the least-squares problem is over-determined. The distinct-channel condition is automatically satisfied in the new formulation because all common factors have been extracted out. Therefore, the focus of the discussion is the input linear complexity.

The theorems and lemmas will be derived for the all-zero system. The proof could be extended to the all-pole system and the pole-zeros system as shown in section 2.2.2 . In the following derivation, L_1 and L_2 denote the order of the distinct dynamics of the two channels respectively, whose definition are as follows:

All-zero system: $L_1 = m_1' + 1, L_2 = m_2' + 1$

All-pole system: $L_1 = n_1' + 1, L_2 = n_2' + 1$

Pole-zero system: $L_1 = n_1' + m_2' + 1 + 1, L_2 = n_2' + m_1' + 1$

L_c denotes one plus the number of zeros in the common dynamics, i.e., $L_c = m_0 + 1$; L_d denotes the maximum order of the distinct dynamics of the two channels, i.e., $L_d = \max(L_1, L_2)$; K denotes the number by which the order of the distinct dynamics is overestimated; L_e denotes the estimated maximum order of the distinct dynamics, i.e.: $L_e = L_d + K$.

3.2.1 Necessary Condition on Input Linear Complexity

The distinct dynamics could not be identified uniquely under the condition stated in the following theorem.

> ***Theorem 2***: Assuming no noise, the MBSI problem with common dynamics does not have a unique solution if $v(n)$ has a linear complexity of order less than L_d.

The proof of Theorem 2 follows the proof of the necessary condition in Theorem 1 given in Appendix A.

3.2.2 Exact Order of Distinct Dynamics is Known

a) Problem Formulation

The output of each channel, $y_i(n)$, is the convolution of the intermediate input, $v(n)$, with the impulse response of the distinct dynamics of the corresponding channel, $h_i'(n)$, i.e.:

$$y_i(k) = [v(k - L_d + 1) \quad \cdots \quad v(k)] \begin{bmatrix} h_i'(L_d) \\ \vdots \\ h_i'(1) \end{bmatrix}, i = 1, 2 \tag{43}$$

Similarly, the intermediate input, $v(n)$, can be written as the convolution of the original input, $u(n)$, with the impulse response of the common dynamics, $h_0(n)$:

$$v(k) = [u(k - L_c + 1) \quad \cdots \quad u(k)] \begin{bmatrix} h_0(L_c) \\ \vdots \\ h_0(1) \end{bmatrix}, i = 1, 2 \tag{44}$$

When L_d is known, $\mathbf{W}_1$ and $\mathbf{W}_2$ are vectors with dimension of $L_d \times 1$. The matrix $\mathbf{Y}$ in eq. (24) is formulated as follows:

$$\begin{aligned} \mathbf{Y}(L_d) &= [\mathbf{Y}_2(L_d), \quad -\mathbf{Y}_1(L_d)] \\ &= [\mathbf{V}(L_d) \cdot \mathbf{H}_2'(L_d), \quad -\mathbf{V}(L_d) \cdot \mathbf{H}_1'(L_d)] \\ &= \mathbf{V}(L_d) \cdot [\mathbf{H}_2'(L_d), \quad -\mathbf{H}_1'(L_d)] \\ &= \{\mathbf{U}(L_d) \cdot \mathbf{H}_0(L_d)\} \cdot [\mathbf{H}_2'(L_d), \quad -\mathbf{H}_1'(L_d)] \end{aligned} \tag{45}$$

where

$$\mathbf{Y}_i(L_d) \equiv \begin{bmatrix} y_i(L_d) & \cdots & y_i(2L_d - 1) \\ \vdots & \ddots & \vdots \\ y_i(N - L_d + 1) & \cdots & y_i(N) \end{bmatrix} : \{(N - 2L_d + 2) \times L_d\}, i = 1, 2 \tag{46}$$

$$\mathbf{H}_i'(L_d) \equiv \begin{bmatrix} h_i'(L_d) & & \\ \vdots & \ddots & \\ h_i'(1) & \cdots & h_i'(L_d) \\ & \ddots & \vdots \\ & & h_i'(1) \end{bmatrix} : \{(2L_d - 1) \times L_d\}, i = 1, 2 \tag{47}$$

$$\mathbf{V}(L_d) \equiv \begin{bmatrix} v(1) & \cdots & v(2L_d - 1) \\ \vdots & \ddots & \vdots \\ v(N - 2L_d + 2) & \cdots & v(N) \end{bmatrix} : \{(N - 2L_d + 2) \times (2L_d - 1)\} \tag{48}$$

$$\mathbf{H}_0(L_d) \equiv \begin{bmatrix} h_0(L_c) & & \\ \vdots & \ddots & \\ \vdots & \cdots & h_0(L_c) \\ \vdots & \cdots & \vdots \\ h_0(1) & \cdots & \vdots \\ & \ddots & \vdots \\ & & h_0(1) \end{bmatrix} : \{(2L_d + L_c - 2) \times (2L_d - 1)\} \tag{49}$$

$$\mathbf{U}(L_d) \equiv \begin{bmatrix} u(2 - L_c) & \cdots & u(2L_d - 1) \\ \vdots & \ddots & \vdots \\ u(N - 2L_d - L_c + 3) & \cdots & u(N) \end{bmatrix} : \{(N - 2L_d + 2) \times (2L_d + L_c - 2)\} \tag{50}$$

b) Solution

Recall that $L_d = \max(L_1, L_2)$. Without loss of generality, assume that $L_d = L_1 = L_2 + \Delta K$. Theorem 3 gives the unique solution to the distinct dynamics identification problem when the order of the dynamics is known. Also given is the sufficient condition on the input linear complexity.

Theorem 3: Assuming that there is no noise and the input $v(n)$ has a linear complexity of order $2L_d - 1$, when L_d is known, the only solution to eq. (24) is $\mathbf{W}_1$ and $\mathbf{W}_2$ whose elements are the coefficients of the following polynomials:

$$\begin{aligned} W_1(z^{-1}) &= \alpha H_1'(z^{-1}) \\ W_2(z^{-1}) &= \alpha H_2'(z^{-1}) \theta_{\Delta K}(z^{-1}) \end{aligned} \tag{51}$$

where α is an arbitrary constant and $\theta_{\Delta K}(z^{-1}) = z^{-\Delta K}$.

Proof:

First, consider the case when $L_d = L_1 = L_2$, i.e., $\Delta K = 0$. Since the input $v(n)$ has a linear complexity of order $2L_d - 1$, the matrix $\mathbf{V}(L_d)$ defined in eq. (48) has full column rank. Therefore,

$$\dim\{\square[\mathbf{Y}(L_d)]\} = \dim\{\square\{[\mathbf{H}_2'(L_d), \quad -\mathbf{H}_1'(L_d)]\}\} \tag{52}$$

where dim{•} denotes the dimension of a matrix • and □[•] denotes the null space of a matrix •. Thus, the solution to eq. (24), $\mathbf{W}_1$ and $\mathbf{W}_2$, must be the solution to the following equation as well:

$$[\mathbf{H}_2'(L_d), \quad -\mathbf{H}_1'(L_d)]\begin{bmatrix}\mathbf{W}_1\\ \mathbf{W}_2\end{bmatrix}=0 \tag{53}$$

This implies that the following relation in the time domain holds:

$$H_2'(z^{-1})W_1(z^{-1}) = H_1'(z^{-1})W_2(z^{-1}) \tag{54}$$

where $W_1(z^{-1})$, $W_2(z^{-1})$, $H_1'(z^{-1})$ and $H_2'(z^{-1})$ are $(L_d - 1)$-th order polynomials. It is obvious that eq. (51) satisfies eq. (54), therefore it is a solution to the problem. This is also the only solution, as proved in the following. From eq. (54), we have:

$$\begin{aligned}\Omega\{H_2'(z^{-1})\} &\subset \Omega\{H_2'(z^{-1})W_1(z^{-1})\}\\ &= \Omega\{H_1'(z^{-1})W_2(z^{-1})\}\\ &= \Omega\{H_1'(z^{-1})\}\cup\Omega\{W_2(z^{-1})\}\end{aligned} \tag{55}$$

According to the distinct-channel condition,

$$\Omega\{H_2'(z^{-1})\}\cap\Omega\{H_1'(z^{-1})\} = \phi \tag{56}$$

Therefore, $\Omega\{H_2'(z^{-1})\}\subset\Omega\{W_2(z^{-1})\}$. But the orders of the two polynomials is the same, thus

$$\Omega\{H_2'(z^{-1})\} = \Omega\{W_2(z^{-1})\} \tag{57}$$

i.e.:

$$W_2(z^{-1}) = \alpha H_2'(z^{-1}) \tag{58}$$

Similarly, we can prove

$$W_1(z^{-1}) = \alpha H_1'(z^{-1}) \tag{59}$$

So $\mathbf{W}_1$ and $\mathbf{W}_2$ given in eq. (58) and (59) are the unique solution to eq. (24) when $\Delta K = 0$.

Now consider the case when $\Delta K \neq 0$. The relation described in eq. (53) still holds in this case except that the matrix $\mathbf{H}_2'(L_d)$ is defined differently from the case when $\Delta K = 0$:

$$\mathbf{H}_2'(L_d)=\begin{bmatrix} & \begin{matrix}0\\ \vdots\\ 0\end{matrix}\ \Big\}\Delta K & \begin{matrix}\ddots & & \\ \vdots & & \\ 0 & \vdots & 0\end{matrix} & & \\ & \begin{matrix}h_2'(L_2)\\ \vdots\\ h_2'(1)\end{matrix}\ \Big\}2L_2+\Delta K-1 & \begin{matrix}\ddots & \vdots & \ddots & \\ \ddots & 0 & \vdots & 0\\ \cdots & h_2'(L_2) & \ddots & \vdots\\ \ddots & \vdots & \ddots & 0\\ & h_2'(1) & \cdots & h_2'(L_2)\\ & & \ddots & \vdots\\ & & & h_2'(1)\end{matrix} & \end{bmatrix} \tag{60}$$

The cross relation in eq. (54) also holds:

$$H_2''(z^{-1})W_1(z^{-1})=H_1'(z^{-1})W_2(z^{-1}) \tag{61}$$

where $W_1(z^{-1})$, $W_2(z^{-1})$, and $H_1'(z^{-1})$ are defined as before and $H_2''(z^{-1})$ defined as an $(L_d 1)$-th order polynomial with coefficients specified by the following vector $\mathbf{h}_2''$:

$$\mathbf{h}_2''=\begin{bmatrix}\underbrace{0\ \cdots\ 0}_{\Delta K} & h_2'(1) & \cdots & h_2'(L_2)\end{bmatrix}^T \tag{62}$$

Therefore, $\Omega\{H_2''(z^{-1})\}$ includes L_2 roots coming from the channel dynamics and ΔK additional roots at the origin. Similarly, eq. (61) requires

$$\begin{aligned}\Omega\{W_1(z^{-1})\}&=\Omega\{H_1'(z^{-1})\}\\ \Omega\{W_2(z^{-1})\}&=\Omega\{H_2''(z^{-1})\}\end{aligned} \tag{63}$$

In other words, the unique solution to eq. (24) when $\Delta K \neq 0$ is:

$$\begin{aligned}W_1(z^{-1})&=\alpha H_1'(z^{-1})\\ W_2(z^{-1})&=\alpha H_2'(z^{-1})z^{-\Delta K}\end{aligned} \tag{64}$$

End of Proof.

3.2.3 Order of Distinct Dynamics is Over-estimated

a) Problem Formulation

When L_d is unknown, an estimated upper limit of the maximum order L_e is given. $\mathbf{W}_1$ and $\mathbf{W}_2$ are vectors with dimension of $L_e \times 1$. The matrix $\mathbf{Y}$ in eq. (24) is formulated as follows:

$$\begin{aligned}\mathbf{Y}(L_e) &= [\mathbf{Y}_2(L_e), \quad -\mathbf{Y}_1(L_e)] \\ &= [\mathbf{V}(L_e)\cdot\mathbf{H}_2'(L_e), \quad -\mathbf{V}(L_e)\cdot\mathbf{H}_1'(L_e)] \\ &= \mathbf{V}(L_e)\cdot[\mathbf{H}_2'(L_e), \quad -\mathbf{H}_1'(L_e)] \\ &= \{\mathbf{U}(L_e)\cdot\mathbf{H}_0(L_e)\}\cdot[\mathbf{H}_2'(L_e), \quad -\mathbf{H}_1'(L_e)]\end{aligned} \tag{65}$$

where

$$\mathbf{Y}_i(L_e) \equiv \begin{bmatrix} y_i(L_e) & \cdots & y_i(2L_e-1) \\ \vdots & \ddots & \vdots \\ y_i(N-L_e+1) & \cdots & y_i(N) \end{bmatrix} : \{(N-2L_e+2)\times L_e\}, i=1,2 \tag{66}$$

$$\mathbf{H}_i'(L_e) \equiv \begin{bmatrix} h_2'(L_d) & & & & & & \\ \vdots & \ddots & & & & & \\ h_2'(1) & \cdots & h_2'(L_d) & & & & \\ & \ddots & \vdots & h_2'(L_d) & & & \\ & & h_2'(1) & \vdots & \ddots & & \\ & & & h_2'(1) & h_2'(L_d) & & \\ & & & & \ddots & \vdots & \\ & & & \underbrace{\qquad\qquad}_{K} & & h_2'(1) & \end{bmatrix} : \{(2L_e-K-1)\times L_e\}, i=1,2 \tag{67}$$

$$\mathbf{V}(L_e) \equiv \begin{bmatrix} v(K+1) & \cdots & v(2L_e-1) \\ \vdots & \ddots & \vdots \\ v(N-2L_e+K+2) & \cdots & v(N) \end{bmatrix} : \{(N-2L_e+2)\times(2L_e-K-1)\} \tag{68}$$

$$\mathbf{H}_0(L_e) \equiv \begin{bmatrix} h_0(L_c) & & & & \\ \vdots & \ddots & & & \\ h_0(1) & \cdots & h_0(L_c) & & \\ & \ddots & \vdots & \ddots & \\ & & h_0(1) & \cdots & h_0(L_c) \\ & & & \ddots & \vdots \\ & & & & h_0(1) \end{bmatrix} \quad (69)$$

$$:\{(2L_e - K + L_c - 2) \times (2L_e - K - 1)\}$$

$$\mathbf{U}(L_e) \equiv \begin{bmatrix} u(K - L_c + 2) & \cdots & u(2L_e - 1) \\ \vdots & \ddots & \vdots \\ u(N - 2L_e + K - L_c + 3) & \cdots & u(N) \end{bmatrix} \quad (70)$$

$$:\{(N - 2L_e + 2) \times (2L_e - K + L_c - 2)\}$$

b) Solution

Similar to the case when L_d is known, assume that $L_d = L_1 = L_2 + \Delta K$. Lemma 3 gives a particular solution to the distinct dynamics identification problem when the order is over-estimated by K.

Lemma 3: Assuming no noise, when L_d is unknown and an estimated upper limit of the maximum order L_e is given, one particular solution to eq. (24) is $\mathbf{W}_1$ and $\mathbf{W}_2$ whose elements are the coefficients of the following polynomials:

$$\begin{aligned} W_1(z^{-1}) &= \alpha H_1'(z^{-1})\theta_1(z^{-1}) \\ W_2(z^{-1}) &= \alpha H_2'(z^{-1})\theta_1(z^{-1})\theta_{\Delta K}(z^{-1}) \end{aligned} \quad (71)$$

where α is an arbitrary constant, $\theta_{\Delta K}(z^{-1}) = z^{-\Delta K}$ and $\theta_1(z^{-1})$ is a polynomial of order K whose roots are at arbitrary locations.

Proof:

A proof of the above lemma is trivial. Plugging $\mathbf{W}_1$ and $\mathbf{W}_2$ given in eq. (71) into eq. (24) gives zero.

End of Proof.

Lemma 4 tells the number of existing solutions for the over-estimation case, which is determined by the dimension of the null space of the matrix $\mathbf{Y}(L_e)$.

Lemma 4: Assuming no noise and the input $v(n)$ has a linear complexity of order $2L_d + K - 1$, $\dim\{\square\,[\mathbf{Y}(L_e)]\} = K+1$.

Proof:

From Lemma 5, we know that when the input $v(n)$ has a linear complexity of order $2L_d + K - 1$, $\mathbf{V}(L_e)$ has full column rank. Therefore,

$$\dim\{\square[\mathbf{Y}(L_e)]\} = \dim\{\square\{[\mathbf{H}_2'(L_e), \quad -\mathbf{H}_1'(L_e)]\}\} \tag{72}$$

From Theorem 3, we know that

$$\dim\{\square[\mathbf{H}_2'(L_d), \quad -\mathbf{H}_1'(L_d)]\} = 1 \tag{73}$$

The null space of $[\mathbf{H}_2'(L_d), \quad -\mathbf{H}_1'(L_d)]$ is spanned by the vector $[\mathbf{h}_1'^{T}, \quad \mathbf{h}_2'^{T}]^T$, i.e.:

$$\begin{bmatrix} h_2'(L_d) & & & -h_1'(L_d) & & \\ \vdots & \ddots & & \vdots & \ddots & \\ h_2'(1) & \cdots & h_2'(L_d) & -h_1'(1) & \cdots & -h_1'(L_d) \\ & \ddots & \vdots & & \ddots & \vdots \\ & & h_2'(1) & & & -h_1'(1) \end{bmatrix} \cdot \begin{bmatrix} h_1'(L_d) \\ \vdots \\ h_1'(1) \\ h_2'(L_d) \\ \vdots \\ h_2'(1) \end{bmatrix} = 0 \tag{74}$$

Notice that $h_1'(1)$ and $h_2'(1)$ cannot be zero at the same time (otherwise, the two channels share a common root at the origin, which contradicts with the distinct-channel condition). Without loss of generality, assume $h_2'(1) \neq 0$. Therefore, the last column in matrix $\mathbf{Y}(L_d)$ is a linear combination of other columns.

Now add one column to $\mathbf{H}_2'(L_d)$ and consider the following matrix:

$$\mathbf{H}'(L_d+1, L_d) = \begin{bmatrix} h_2'(L_d) & & & & -h_1'(L_d) & & \\ \vdots & \ddots & & & \vdots & \ddots & \\ h_2'(1) & \cdots & h_2'(L_d) & & -h_1'(L_d) & \cdots & -h_1'(L_d) \\ & \ddots & \vdots & h_2'(L_d) & & \ddots & \vdots \\ & & h_2'(1) & \vdots & & & -h_1'(1) \\ & & & h_2'(1) & & & 0 \end{bmatrix} \tag{75}$$

It is obvious that the additional column is independent because $h_2'(1) \neq 0$. Thus,

$$\dim\{\square[\mathbf{H}'(L_d+1, L_d)]\} = \dim\{\square[\mathbf{H}'(L_d, L_d)]\} = 1 \tag{76}$$

Similarly, adding more columns to $\mathbf{H}_2'(L_d)$ does not change the dimension of the null space of the matrix, i.e.:

$$\dim\{\square[\mathbf{H}'(L_d+K, L_d)]\} = \dim\{\square[\mathbf{H}'(L_d, L_d)]\} = 1 \tag{77}$$

where

$$\mathbf{H}'(L_d+K, L_d) = \begin{bmatrix} h_2'(L_d) & & & & & -h_1'(L_d) & \\ \vdots & \ddots & & & & \vdots & \ddots & \\ h_2'(1) & \cdots & h_2'(L_d) & & & -h_1'(1) & \cdots & -h_1'(L_d) \\ & \ddots & \vdots & h_2'(L_d) & & & \ddots & \vdots \\ & & h_2'(1) & \vdots & \ddots & & & -h_1'(1) \\ & & & h_2'(1) & h_2'(L_d) & & & 0 \\ & & & & \ddots & \vdots & & \vdots \\ & & & & h_2'(1) & 0 & & 0 \\ & & & \underbrace{\qquad\qquad}_{K} & & & & \end{bmatrix} \begin{matrix} \\ \\ \\ \\ \\ \\ \\ \} K \end{matrix} \tag{78}$$

Now add one more column to $\mathbf{H}_1'(L_d)$ and consider the following matrix:

$$\mathbf{H}'(L_d+K, L_d+1) = \begin{bmatrix} h_2'(L_d) & & & & & -h_1'(L_d) & & \\ \vdots & \ddots & & & & \vdots & \ddots & \\ h_2'(1) & \cdots & h_2'(L_d) & & & -h_1'(1) & \cdots & -h_1'(L_d) \\ & \ddots & \vdots & h_2'(L_d) & & & \ddots & \vdots & -h_1'(L_d) \\ & & h_2'(1) & \vdots & \ddots & & -h_1'(1) & \vdots \\ & & & h_2'(1) & h_2'(L_d) & & 0 & -h_1'(1) \\ & & & & \ddots & \vdots & \vdots & \vdots \\ & & & & h_2'(1) & & 0 & 0 \end{bmatrix} \tag{79}$$

Recall that the last column in matrix $\mathbf{Y}(L_d)$ is a linear combination of other columns. As a result, the last column in $\mathbf{H}'(L_d+K, L_d+1)$ is a linear combination of other columns as well. From linear algebra [14], we know that if b belongs to the column space of a matrix A, then

$$\text{rank}[A \mid b] = \text{rank}[A] \tag{80}$$

Therefore, rank{ $\mathbf{H}'(L_d+K, L_d+1)$ } = rank { $\mathbf{H}'(L_d+K, L_d)$ }, i.e.:

$$\dim\{\square[\mathbf{H}'(L_d+K,L_d+1)]\}=\dim\{\square[\mathbf{H}'(L_d+K,L_d)]\}+1=2 \tag{81}$$

Similarly,

$$\dim\{\square[\mathbf{H}'(L_d+K,L_d+2)]\}=\dim\{\square[\mathbf{H}'(L_d+K,L_d)]\}+2=3 \tag{82}$$

...

$$\dim\{\square[\mathbf{H}'(L_d+K,L_d+K)]\}=\dim\{\square[\mathbf{H}'(L_d+K,L_d)]\}+K=K+1 \tag{83}$$

Consequently,

$$\dim\{\square[\mathbf{Y}(L_e)]\}=K+1 \tag{84}$$

Therefore, when the input $u(n)$ has a linear complexity of order $2L_d + L_c + K - 2$, $\dim\{\square[\mathbf{Y}(L_e)]\}=K+1$.

End of Proof.

Theorem 4 gives the sufficient condition on the input linear complexity and proves that the particular solution given in Lemma 3 is also the unique solution to the distinct dynamics identification problem when the order of the dynamics is over-estimated.

Theorem 4: Assuming no noise and the input $v(n)$ has a linear complexity of order $2L_d + K - 1$, when L_d is unknown and an estimated upper limit of the maximum order L_e is given, the only solution to eq. (24) is the one that is of the form given in eq. (71).

Proof:

From Lemma 3, the K roots of θ_1, which can be chosen at any arbitrary locations, together with the scalar factor α, imply an (K+1)-dimension space $\mathbf{W}$ for the solution to eq. (24). There is a one-to-one correspondence between the (K+1) parameters and the vectors in $\mathbf{W}$. On the other hand, the dimension of the null space of $\mathbf{Y}(L_e)$ determines the number of solutions to eq. (24). From Lemma 4, we know that the input $v(n)$ has a linear complexity of order $2L_d + K - 1$, $\dim\{\square[\mathbf{Y}(L_e))]\} = K+1$. Therefore the null space of $\mathbf{Y}(L_e)$ must be $\mathbf{W}$, thus $\mathbf{W}_1$ and $\mathbf{W}_2$ given in eq. (71) are the only solution to eq. (24) when the input $v(n)$ has a linear complexity of order $2L_d + K - 1$.

End of Proof.

3.2.4 Relationship Between the Linear Complexity of $u(n)$ and $v(n)$

In section 3.2.1 , 3.2.2 and 3.2.3 , necessary and sufficient conditions for the distinct dynamics identification were derived in terms of the linear complexity condition of the intermediate input $v(n)$. Since this is a variable that we created, it does not necessarily have any physical meaning. It is desired to translate the condition on $v(n)$ to the linear complexity condition on a physical variable, such as the original input $u(n)$, which is the focus of this section.

a) All-zero System (MA model)

When the common dynamics are represented by an MA model,

$$H_0(z^{-1}) = \frac{V(z^{-1})}{U(z^{-1})} = N_0(z^{-1}) = b_{0,0} + b_{0,1}z^{-1} + \ldots + b_{0,m_0}z^{-m_0} \tag{85}$$

The difference equation describing the relation between the intermediate input $v(n)$ and the original input $u(n)$ is:

$$v(k) = [u(k-m_0) \quad \cdots \quad u(k)]\begin{bmatrix} b_{0,m_0} \\ \vdots \\ b_{0,0} \end{bmatrix} \tag{86}$$

The following lemma describes the relationship between the linear complexity of the original input $u(n)$ and that of the intermediate input $v(n)$.

> ***Lemma 5***: For the common dynamics in the two-channel system shown in Figure 9, if $u(n)$ has a linear complexity of order $p+m_0$, then $v(n)$ at least has a linear complexity of order p; if $v(n)$ has a linear complexity of order less than p, then $u(n)$ has a linear complexity of order less than $p+m_0$.

Proof:

According to eq. (86), the input-output relation of the common dynamics gives:

$$\mathbf{V} = \mathbf{U} \cdot \mathbf{H}_0 \tag{87}$$

where

$$\mathbf{V} \equiv \begin{bmatrix} v(1) & \cdots & v(p) \\ \vdots & \ddots & \vdots \\ v(N-p+1) & \cdots & v(N) \end{bmatrix} : \{(N-p+1)\times p\} \tag{88}$$

$$\mathbf{U} \equiv \begin{bmatrix} u(1-m_0) & \cdots & u(0) & u(1) & \cdots & u(p) \\ \vdots & \ddots & \vdots & \vdots & \ddots & \vdots \\ u(N-p-m_0+1) & \cdots & u(N-p+1) & u(N-p+2) & \cdots & u(N) \end{bmatrix} : \{(N-p+1)\times(p+m_0)\} \tag{89}$$

$$\mathbf{H}_0 \equiv \begin{bmatrix} b_{0,m_0} & \ddots & & \\ \vdots & & \ddots & \\ b_{0,0} & \ddots & & b_{0,m_0} \\ & & \ddots & \vdots \\ & & & b_{0,0} \end{bmatrix} : \{(p+m_0)\times p\} \tag{90}$$

If $u(n)$ has a linear complexity of order $p+m_0$, $\mathbf{U}$ has full column rank according to Lemma 1. In addition, $\mathbf{H}_0$ has full column rank because of the band-diagonal structure. Let h_i denote the i^{th} column of $\mathbf{H}_0$, and v_i denote the i^{th} column of $\mathbf{V}$. They satisfy the following relation:

$$v_i = \mathbf{U} \cdot h_i, i = 1, 2, ..., p \tag{91}$$

Assume that rank($\mathbf{V}$) = p-1, i.e.: there is at least one dependent column in $\mathbf{V}$. Without loss of generality, assume that v_p is dependent, i.e.:

$$v_p = c_1 v_1 + ... + c_{p-1} v_{p-1} \tag{92}$$

Substituting eq. (91) into eq. (92):

$$\mathbf{U} \cdot h_p = c_1 \mathbf{U} \cdot h_1 + ... + c_{p-1} \mathbf{U} \cdot h_{p-1} \tag{93}$$

Rearranging eq. (93):

$$\mathbf{U} \cdot (h_p - c_1 h_1 - ... - c_{p-1} h_{p-1}) = 0 \tag{94}$$

Since $\mathbf{U}$ has full column rank, its null space must be zero, i.e.:

$$h_p - c_1 h_1 - ... - c_{p-1} h_{p-1} = 0 \tag{95}$$

This implies that there is at least one dependent column in $\mathbf{H}_0$, which contradicts the condition that $\mathbf{H}_0$ has full column rank. Therefore, $\mathbf{V}$ must has full column rank, which implies that $v(n)$ has a linear complexity order p.

If $v(n)$ has a linear complexity of order less than p, there exists at least one non-zero column vector x, such that $\mathbf{V}x = 0$. Right multiplying vector x to both sides of eq. (87) yields:

$$\mathbf{V} \cdot x = \mathbf{U} \cdot (\mathbf{H}_0 x) = 0 \tag{96}$$

Since $\mathbf{H}_0$ has full column rank, the column vector $\mathbf{H}_0 x \neq 0$. Therefore, there exist at least one non-zero vector $y = \mathbf{H}_0 x$, such that $\mathbf{U}y = 0$. Therefore, $\mathbf{U}$ does not have full column rank, i.e., $u(n)$ has a linear complexity of order less than $p + m_0$.

End of Proof.

b) All-pole System (AR model)

When the common dynamics are presented by an AR model,

$$H_0(z^{-1}) = \frac{V(z^{-1})}{U(z^{-1})} = \frac{1}{D_0(z^{-1})} = \frac{1}{a_{0,0} + a_{0,1}z^{-1} + \ldots + a_{0,n_0}z^{-n_0}} \tag{97}$$

The difference equation describing the relation between the intermediate input $v(n)$ and the original input $u(n)$ is:

$$u(k) = [v(k - n_0) \quad \cdots \quad v(k)] \begin{bmatrix} a_{0,n_0} \\ \vdots \\ a_{0,0} \end{bmatrix} \tag{98}$$

The following lemma describes the relationship between the linear complexity of the original input $u(n)$ and that of the intermediate input $v(n)$.

Lemma 6: For the common dynamics in the two-channel system shown in Figure 9, if $u(n)$ has a linear complexity of order p, then $v(n)$ has a linear complexity of at least order p and at most order $p+n_0$.

Proof:

According to eq. (98), the input-output relation of the common dynamics gives:

$$\mathbf{U} = \mathbf{V} \cdot \mathbf{H}_0 \tag{99}$$

where

$$\mathbf{U} \equiv \begin{bmatrix} u(1) & \cdots & u(p) \\ \vdots & \ddots & \vdots \\ u(N-p+1) & \cdots & u(N) \end{bmatrix} : \{(N-p+1)\times p\} \tag{100}$$

$$\mathbf{V} \equiv \begin{bmatrix} v(1-n_0) & \cdots & v(0) & v(1) & \cdots & v(p) \\ \vdots & \ddots & \vdots & \vdots & \ddots & \vdots \\ v(N-p-n_0+1) & \cdots & v(N-p+1) & v(N-p+2) & \cdots & v(N) \end{bmatrix} : \{(N-p+1)\times(p+n_0)\} \tag{101}$$

$$\mathbf{H}_0 \equiv \begin{bmatrix} a_{0,n_0} & \ddots & & \\ \vdots & & \ddots & \\ a_{0,0} & \ddots & & a_{0,n_0} \\ & & \ddots & \vdots \\ & & & a_{0,0} \end{bmatrix} : \{(p+n_0)\times p\} \tag{102}$$

If $u(n)$ has a linear complexity of order p, $\mathbf{U}$ has full column rank according to Lemma 1. In addition, $\mathbf{H}_0$ has full column rank because of the band-diagonal structure. According to the Sylvester inequality,

$$\text{rank}(\mathbf{V}) + \text{rank}(\mathbf{H}_0) - (p+n_0) \le \text{rank}(\mathbf{U}) \le \text{rank}(\mathbf{V}) \tag{103}$$

i.e.:

$$p \le \text{rank}(\mathbf{V}) \le p + n_0 \tag{104}$$

Therefore, $v(n)$ has a linear complexity of at least order p and at most order $p+n_0$.

End of Proof.

c) Pole-zero System (ARMA model)

When the common dynamics are presented by an ARMA model,

$$H_0(z^{-1}) = \frac{V(z^{-1})}{U(z^{-1})} = \frac{N_0(z^{-1})}{D_0(z^{-1})} = \frac{b_{0,0} + b_{0,1}z^{-1} + \ldots + b_{0,m_0}z^{-m_0}}{a_{0,0} + a_{0,1}z^{-1} + \ldots + a_{0,n_0}z^{-n_0}} \tag{105}$$

The difference equation describing the relation between the intermediate input $v(n)$ and the original input $u(n)$ is:

$$[v(k-n_0) \quad \cdots \quad v(k)]\begin{bmatrix} a_{0,n_0} \\ \vdots \\ a_{0,0} \end{bmatrix} = [u(k-m_0) \quad \cdots \quad u(k)]\begin{bmatrix} b_{0,m_0} \\ \vdots \\ b_{0,0} \end{bmatrix} \tag{106}$$

It is clear from Lemma 5 and Lemma 6, the AR part will not reduce the linear complexity of the input. Therefore the relation between the linear complexity of $u(n)$ and $v(n)$ is the same as the relation for the all-zero system.

Lemma 7: For the common dynamics in the two-channel system shown in Figure 9, if $u(n)$ has a linear complexity of order $p+m_0$, then $v(n)$ at least has a linear complexity of order p; if $v(n)$ has a linear complexity of order less than p, then $u(n)$ has a linear complexity of order less than $p+m_0$.

d) Summary

The relationship between the linear complexity of the original input $u(n)$ and that of the intermediate input $v(n)$ for different models, described in Lemma 3, Lemma 4, and Lemma 5 respectively, are summarized in the following inequalities:

$$\text{MA Model:} \quad p_u - m_0 \le p_v \le p_u \tag{107}$$

$$\text{AR Model:} \quad p_u \le p_v \le p_u + n_0 \tag{108}$$

$$\text{ARMA Model:} \quad p_u - m_0 \le p_v \le p_u + n_0 \tag{109}$$

where p_u and p_v denotes the number of mode in $u(n)$ and $v(n)$ respectively.

3.2.5 Implementation of Channel Order Estimation

When the channel orders are overestimated, the solutions to eq. (24), $W_1(z^{-1}), W_2(z^{-1})$ given in eq. (71), are polynomials with higher orders than $H_1'(z^{-1}), H_2'(z^{-1})$, as explained in section 3.2.3 . The locations of the extraneous roots of $W_1(z^{-1}), W_2(z^{-1})$ have the following property: the two channels have exactly the same extraneous roots, except that the one with the larger order has all of its additional extraneous roots at the origin. In the noiseless case, the matrix $\mathbf{Y}(L_e)$ defined in eq. (65)

has K zero singular values. If there is additive noise, then $\mathbf{Y}(L_e)$ is of full rank. However, for reasonably large N, it can be shown [10] that the K+1 smallest eigenvalues are close to σ_n, which is the square root of the noise power density. These singular values are usually called noise singular values. Therefore, by checking how many smaller singular values of $\mathbf{Y}(L_e)$ are close to one another, we can detect K+1 or detect L_d since L_e is known. More objective criteria such as MDL [12], AIC [12], and other detection methods [15][16] can also be used to detect L_d.

The procedure for channel order estimation is the following:

- Overestimate the channel order as L_e;
- Formulate the matrix $\mathbf{Y}(L_e)$ from the signals observed;
- Calculate the singular values of $\mathbf{Y}(L_e)$;
- Based on the knowledge of the noise level, estimate how many smaller singular values are the noise singular value and detect the maximum channel order L_d;
- Use the estimated L_d to formulate $\mathbf{Y}(\hat{L}_d)$;
- Obtain the least-squares estimation of the distinct dynamics from the singular vector corresponding to the smallest singular value of $\mathbf{Y}(\hat{L}_d)$.

3.3 Common Dynamics Identification

Based on the above derivation, the distinct dynamics can be identified by solving eq. (24) when the input has sufficient linear complexity and there are enough output samples. The intermediate input $v(n)$ can then be identified. To solve the common dynamics from $v(n)$, we explore the zero-input response of the system. Consider the common dynamics:

$$\begin{aligned} \mathbf{x}(n+1) &= \mathbf{F}\mathbf{x}(n) + \mathbf{G}u(n) \\ v(n) &= \mathbf{J}\mathbf{x}(n) \end{aligned} \tag{110}$$

where $\mathbf{x}$ is the array of state variables, $\mathbf{F}$, $\mathbf{G}$, and $\mathbf{J}$ are matrices with proper dimensions. The response of the system $v(n)$ consists of two components: the zero-input response and the zero-state response [13]. The zero-input response is the response due to the non-zero initial condition when the input is zero. The zero-state response is the response due to the input when the initial condition is zero. Letting $V(z^{-1})$ and $U(z^{-1})$ be the z-transform of the corresponding signals, they have the relation:

$$V(z^{-1}) = [\mathbf{J}z(z\mathbf{I} - \mathbf{F})^{-1}]\mathbf{x}(0) + [\mathbf{J}(z\mathbf{I} - \mathbf{F})^{-1}\mathbf{G}]U(z^{-1}) \tag{111}$$

where $\mathbf{x}(0)$ is the initial condition of the state variables. The two terms in eq. (111) correspond to the zero-input response and the zero-state response respectively. If we require that the input be zero for certain time, the second term disappears. Then the modes in the common dynamics can be identified from $v(n)$ given that they have been excited. Since the zero-input response does not contain the information about the matrix $\mathbf{G}$, i.e., the information about the zero locations, only the pole locations can be obtained from the zero-input response.

If the common dynamics between $u(n)$ and $v(n)$ are described by the following ARMA model:

$$v(n) = \sum_{k=0}^{m_0} b_{0,k}u(n-k) + \sum_{k=1}^{n_0} a_{0,k}v(n-k) \tag{112}$$

the moving average coefficients, $b_{0,k}$, $k = 1, \ldots, m_0$, will disappear when $u(n)$ is zero. Only the auto-regressive coefficients, $a_{0,k}$, $k = 1, \ldots, n_0$, could be identified from the zero-input dynamics by solving the following linear equations:

$$\begin{bmatrix} v(t_0) \\ v(t_0+1) \\ \vdots \\ v(N) \end{bmatrix} = \begin{bmatrix} v(t_0-1) & \cdots & v(t_0-n_0) \\ v(t_0) & \cdots & v(t_0-n_0+1) \\ \vdots & \ddots & \vdots \\ v(N-1) & \cdots & v(N-n_0) \end{bmatrix} \begin{bmatrix} a_{0,1} \\ a_{0,2} \\ \vdots \\ a_{0,n_0} \end{bmatrix} \tag{113}$$

where $u(n) = 0$ for $n = t_0, \ldots, N$.

3.4 Intermediate Input Identification Approach

Based on the discussion in section 3.2 and 3.3, the intermediate input identification approach is developed to solve the MBSI problem when common dynamics are present in two steps. The first step in the two-step procedure is to solve the distinct dynamics from the outputs. It has been proven in section 3.2 that the distinct dynamics can be uniquely solved up to a scalar factor from the outputs even when common dynamics are present. The second step is to identify the common dynamics from the intermediate variable $v(n)$ by exploiting the zero-input response. The key concept in the IIID approach is to treat the common dynamics as part of the input. We bundle the common dynamics and the input together and treat the new intermediate variable $v(n)$ as the input to the new

multi-channel system that has no common factor. It is named the intermediate input identification approach since the intermediate variable, which is a filtered input with the common dynamics, plays a pivotal role for dividing the blind identification problem into two executable steps.

The flow chart of the approach is shown in Figure 10. The procedure of the approach is the following:

- Identify the distinct dynamics from the outputs y_1, y_2 using existing MBSI algorithms;
- Estimate the intermediate variable $v(n)$ by deconvolving the estimated distinct dynamics from the outputs;
- Identify the common dynamics from the intermediate input $v(n)$;
- Estimate the input $u(n)$ by deconvolving the estimated dynamics from the outputs.

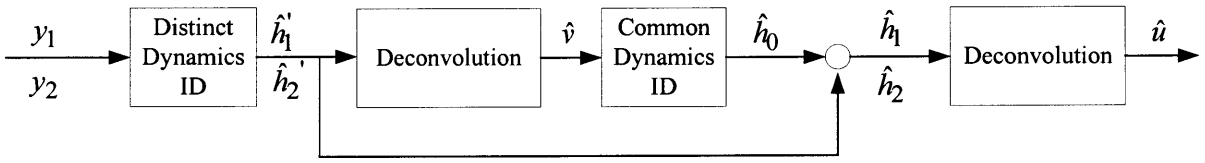

Figure 10. Flow Chart of Intermediate Input ID Approach

In summary, the IIID approach reformulates the MBSI problems with common dynamics by treating the common dynamics as part of the input. It first solves the distinct dynamics of each channel and identifies the intermediate variable. Then it solves the common dynamics by exploring the zero-input response and ultimately recovers the input. Combining the requirements for the distinct dynamics identification and the common dynamics identification, the system has to satisfy the following conditions to be identifiable:

- The output must have enough samples available.
- The intermediate input $v(n)$ must excite all the modes in the distinct dynamics.
- The original input $u(n)$ must excite all the modes in the common dynamics.
- The input must be zero for a sufficiently long period.
- No common zeros are present.

3.5 Numerical Simulations

A few numerical examples are given in this section to illustrate the theory developed in the previous sections.

3.5.1 Relationship between Linear Complexity of $u(n)$ and $v(n)$

This example is to illustrate the relationship between the linear complexity of the original input and that of the intermediate input given in the inequalities (107), (108) and (109). Original input used in this example is $\mathbf{u}(n)=[1\,2\,3\,4\,5\,6\,7\,8\,9\,10\,11]^T$. The modes in $u(n)$ are characterized by the null space of the matrix $U(3)$:

$$U(3)=\begin{bmatrix}1 & 2 & 3\\ 2 & 3 & 4\\ \vdots & \ddots & \vdots\\ 9 & 10 & 11\end{bmatrix} \tag{114}$$

The polynomial characterizing the modes is $1\text{-}2z+z^2$. The two modes in the original input $u(n)$ are thus $z = 1$ and $z = 1$.

a) Case 1: MA model without Pole-zero Cancellation

The common dynamics are described by the MA model $H_0(z^{-1})=1+z^{-1}$. The zero of $H_0(z^{-1})$ is z = -1, which is different from the modes in $u(n)$. The intermediate input generated by the common dynamics is $\mathbf{v}(n)=[1,3,5,7,9,11,13,15,17,19,21]^T$. There are two modes in $v(n)$, based on the same calculation as defined in Lemma 1.

Linear Complexity: $p_u = 2, p_v = 2$.

b) Case 2: MA model with Pole-zero Cancellation

The common dynamics are described by the MA model $H_0(z^{-1})=1-z^{-1}$. The zero of $H_0(z^{-1})$ is z = 1, which coincides with on of the modes in $u(n)$. The intermediate input generated by the common dynamics is $\mathbf{v}(n)=[1,1,1,1,1,1,1,1,1,1,1]^T$. There are two modes in $v(n)$, based on the same calculation as defined in Lemma 1.

Linear Complexity: $p_u = 2, p_v = 1$.

c) Case 3: AR model

The common dynamics are described by the AR model $H_0(z^{-1}) = \frac{1}{1+z^{-1}}$. The pole of $H_0(z^{-1})$ is $z = 1$. The intermediate input generated by the common dynamics is $\mathbf{v}(n) = [1, 3, 6, 10, 15, 21, 28, 36, 45, 55, 66]^T$. There are three modes in $v(n)$, based on the same calculation as defined in Lemma 1.

Linear Complexity: $p_u = 2, p_v = 3$.

d) Case 4: ARMA model without Pole-zero Cancellation

The common dynamics are described by the AR model $H_0(z^{-1}) = \frac{1+z^{-1}}{1+z^{-1}+z^{-2}}$. The zero of $H_0(z^{-1})$ is $z = -1$ and the poles are $z = -0.5 \pm 0.866i$. The intermediate input generated by the common dynamics is $\mathbf{v}(n) = [1, 2, 2, 3, 4, 4, 5, 6, 6, 7, 8]^T$. There are four modes in $v(n)$, based on the same calculation as defined in Lemma 1.

Linear Complexity: $p_u = 2, p_v = 4$.

e) Case 5: ARMA model with Pole-zero Cancellation

The common dynamics are described by the AR model $H_0(z^{-1}) = \frac{1-z^{-1}}{1+z^{-1}+z^{-2}}$. The zero of $H_0(z^{-1})$ is $z = 1$ and the poles are $z = -0.5 \pm 0.866i$. The intermediate input generated by the common dynamics is $\mathbf{v}(n) = [1, 0, 0, 1, 0, 0, 1, 0, 0, 1, 0]^T$. There are four modes in $v(n)$, based on the same calculation as defined in Lemma 1.

Linear Complexity: $p_u = 2, p_v = 3$.

f) Summary

In summary, the zeros in the common dynamics will cancel out the modes in the original input when they coincide with the modes in the original input, while the poles in the common dynamics enrich the original input.

3.5.2 Distinct Dynamics Identification

This example is to illustrate the theorems proven in section 3.2.2 and 3.2.3 . Case 1 and 2 demonstrate the example of an FIR system. Case 3 and 4 demonstrate the example of an IIR system.

a) Case 1: FIR with Known Channel Order

The two-channel system used in Case 1 and Case 2 has finite impulse responses, which are given in Table 1. The impulse responses of the distinct dynamics of the two channels are given in Table 2. The impulse response of the common dynamics is $h_0 = [1, 0.5]^T$. The parameters in this example are the following: $L_1 = 5, L_2 = 3, \Delta K = 2, K = 0\ L_d = 5$. Figure 11 depicts the zero locations of the two channels, where O denotes the zeros of channel 1 and □ denotes the zeros of channel 2. Notice that there is one common zero shared by both channels. Figure 12 and Figure 13 depict the estimated zero locations of the two channels, where ∇ denotes the zeros of channel 1 and Δ denotes the zeros of channel 2. Notice that all the distinct zeros of the two channels are identified uniquely. In addition, there are two extraneous roots in the estimation of channel 2. This is attributed to the order difference between the two channels. Figure 14 plots the singular values of $\mathbf{Y}(L_d)$ in descending order. It is noted that when the maximum channel order is known, there is only one zero singular value. Figure 15 plots the true (left) and the estimated (right) impulse responses of the distinct dynamics of the two channels. The estimation perfectly recovers the true response except the scalar factor, which is the same for both channels.

Table 1: Impulse Responses of the Two Channels for Case 1 and 2

n	1	2	3	4	5	6
$h_1(n)$	1	-0.5	0.5	-0.5	0.5	0.5
$h_2(n)$	1	1.5	1.5	0.5	0	0

Table 2: Impulse Responses of the Distinct Dynamics of the Two Channels for Case 1 and 2

n	1	2	3	4	5
$h_1'(n)$	1	-1	1	-1	1
$h_2'(n)$	1	1	1	0	0

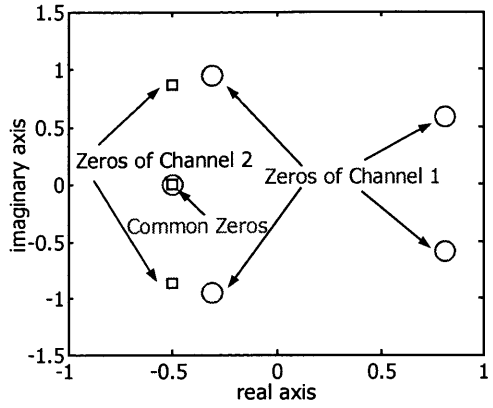

Figure 11. Zero Locations of the Two-channel System for Case 1 and Case 2

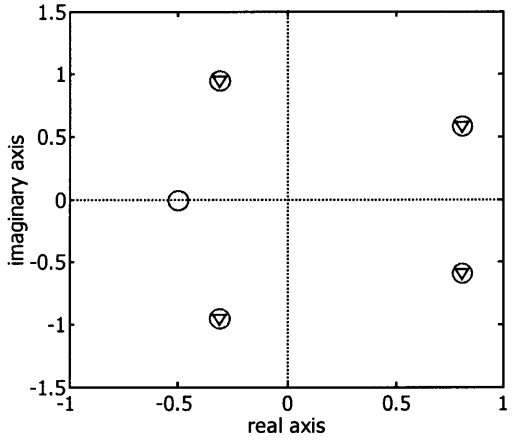

Figure 12. Distinct Channel Dynamics Case 1: Estimated vs. Real Roots of Channel 1

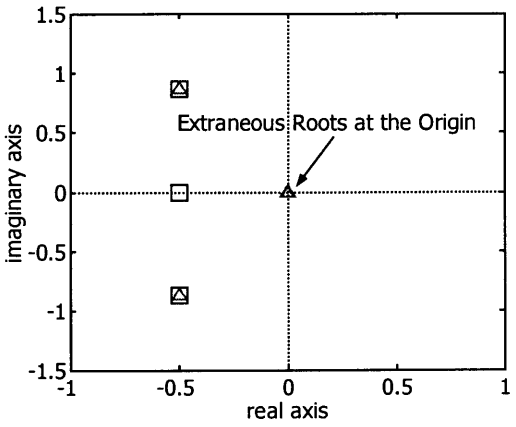

Figure 13. Distinct Channel Dynamics Case 1: Estimated vs. Real Roots of Channel 2

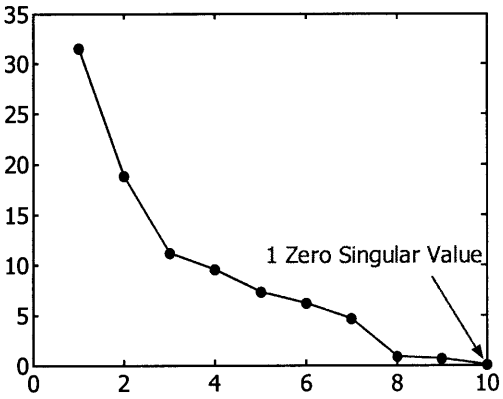

Figure 14. Distinct Channel Dynamics Case 1: Singular Values of Matrix Y in Descending Order

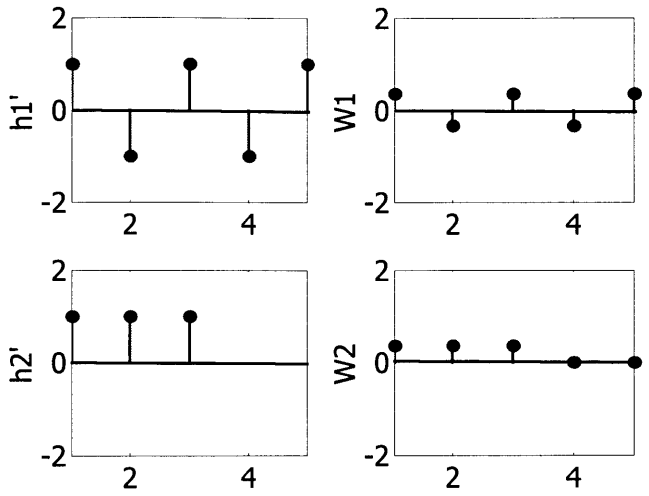

Figure 15. Distinct Channel Dynamics Case 1: Estimated vs. Real Impulse Responses

b) Case 2: FIR with Unknown Channel Order

The same FIR two-channel system is used in this case except the channel order is overestimated by 3. The parameters in this example are the following: $L_1 = 5, L_2 = 3, \Delta K = 2, K = 3, L_e = 8$. Figure 16 and Figure 17 depict the estimated zero locations of the two channels. Notice that again all the distinct zeros of the two channels are identified uniquely and there are two extraneous roots in the estimation of channel 2 due to the order difference. In addition, there are three extraneous roots in both channels. These are the roots due to overestimation. Their locations are irrelevant to the dynamics of the system. Figure 18 compares the estimation of the two channels. Note that the three extraneous roots are at the same locations. Figure 19 plots the singular values of $\mathbf{Y}(L_e)$ in descending order. In this case, there are three additional zero singular values due to order overestimation. Based on the number of zero singular values and the extraneous roots, the channel order can be updated and the matrix $\mathbf{Y}(\hat{L}_d)$ will be reformulated.

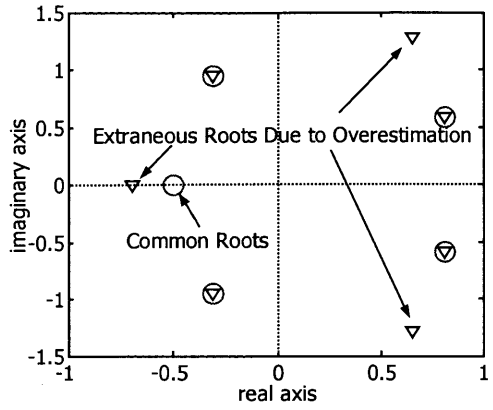

Figure 16. Distinct Channel Dynamics Case 2: Estimated vs. Real Roots of Channel 1

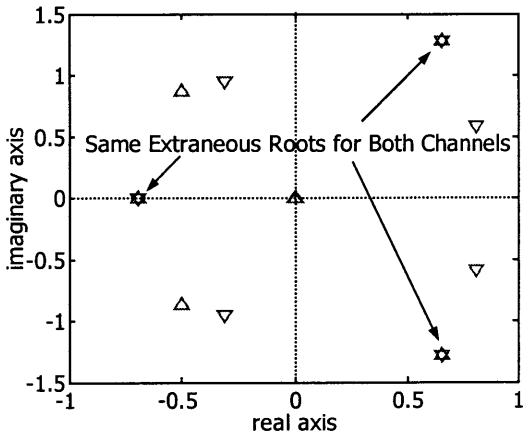

Figure 18. Distinct Channel Dynamics Case 2: Comparison of Channel 1 and 2

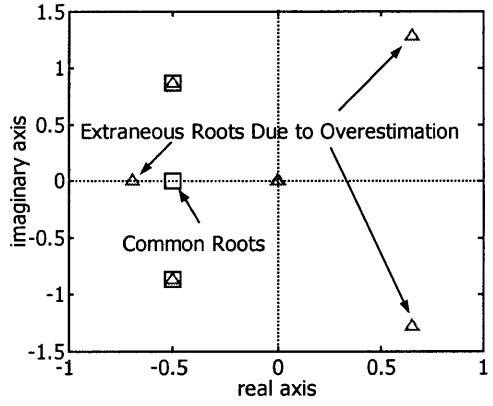

Figure 17. Distinct Channel Dynamics Case 2: Estimated vs. Real Roots of Channel 2

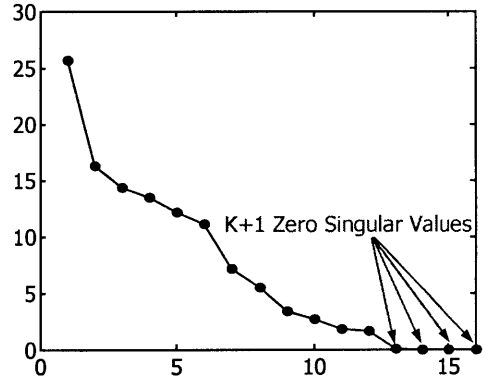

Figure 19. Distinct Channel Dynamics Case 2: Singular Values of Matrix Y in Descending Order

c) Case 3: IIR

Similar simulations were conducted on a three-channel system, where each channel has an IIR. Table 3 shows the transfer functions and the pole and zero locations of the common dynamics and distinct dynamics. Remember that a two-step procedure is needed to identify a system with IIRs, as explained in section.2.1.3 . Figure 20 and Figure 21 depict the result of the first step when the channel orders are known and unknown respectively, where O denotes the true roots and × denotes the estimation. Notice that the distinct roots of each channel are identified accurately. No information on the common dynamics is derived from distinct dynamics identification. When the

channel orders are overestimated (by 4 in this case), all the extraneous roots are at the same locations for both channels.

Table 3: Three-Channel System for Case 3 and 4

	Transfer Function	Poles	Zeros
$H_0(z^{-1})$	$\frac{1}{1+0.64z^{-2}}$	$0.8i$ $-0.8i$	
$H_1'(z^{-1})$	$\frac{2-2z^{-1}+z^{-2}}{1+1.4z^{-1}+0.58z^{-2}}$	$-0.7-0.3i$ $-0.7+0.3i$	$0.5-0.5i$ $0.5+0.5i$
$H_2'(z^{-1})$	$\frac{3+3z^{-1}+1.5z^{-2}}{1-0.6z^{-1}+0.58z^{-2}}$	$0.3-0.7i$ $0.3+0.7i$	$-0.5-0.5i$ $-0.5+0.5i$
$H_3'(z^{-1})$	$\frac{4+0.36z^{-2}}{1+0.36z^{-2}}$	$0.6i$ $-0.6i$	$0.3i$ $-0.3i$

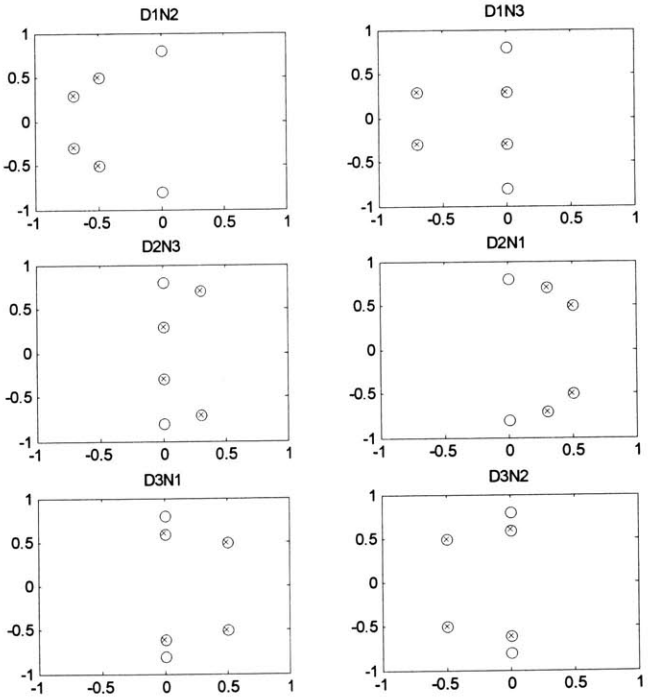

Figure 20. Distinct Channel Dynamics Case 3: Estimated vs. Real Channel Roots When Channel Orders are Known

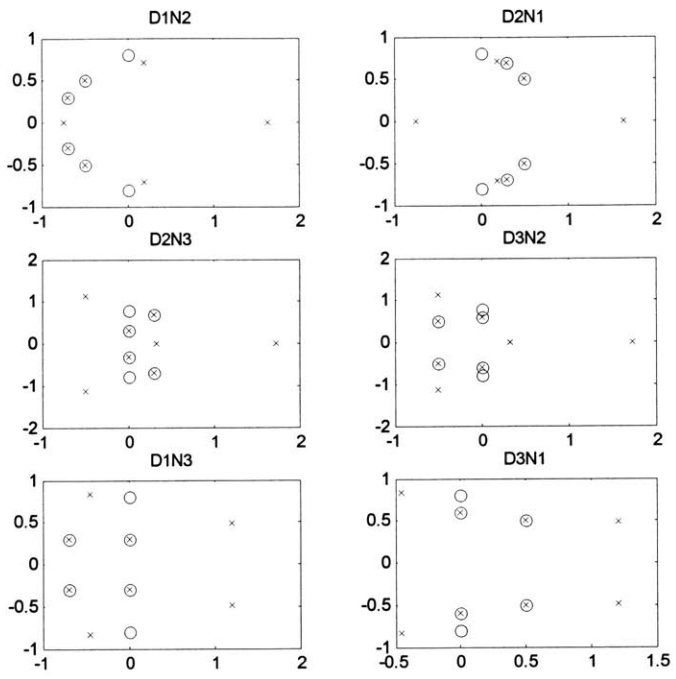

Figure 21. Distinct Channel Dynamics Case 4: Estimated vs. Real Channel Roots When Channel Orders are Unknown

3.5.3 Summary

The distinct dynamics in the multi-channel system can be identified even when common dynamics are present. The estimated roots are classified into three groups:

- Distinct roots of the two channels indicate the distinct dynamics of each channel;
- Roots at the origin in one channel indicate that channel has a lower order than the other channel;
- Same roots in both channels indicate that the channel orders are overestimated; these extraneous roots due to overestimation can be removed through singular value decomposition.

Chapter 4 Application to Central Hemodynamic Monitoring

Chapter 3 developed the IIID approach for the MBSI problem with common dynamics. This chapter will focus on how it is applied to central hemodynamic monitoring. First, it is noted from a review of the anatomy of systemic circulation that the arterial system has a structure that is topologically similar to the wireless communication system introduced in Chapter 1. The idea of modeling the arterial system as a multi-channel system will then be proposed. Second, physiology of systemic circulation will be reviewed, with a concentration on the cardiac cycle and the determinants of arterial blood pressure. These determinants will be classified into three groups, each of which will be modeled as the input, the common dynamics and the distinct dynamics in the multi-channel system. Next, the identifiability conditions for the arterial system will be discussed. In particular, the zero-input condition and the input-linear-complexity condition will be examined. Finally, practical implementation of channel order estimation will be presented.

4.1 Modeling the Arterial System as a Multi-channel System

4.1.1 Anatomy of Systemic Circulation

The circulatory system is composed of an arborizing series of multi-branched conduits arranged in series and in parallel, as illustrated in Figure 22. All systemic arteries branch from the aorta, an elastic vessel about one inch in diameter [18]. It begins at the left ventricle and contains a valve at its origin, the aortic semilunar valve, which prevents backflow of blood into the left ventricle during the ventricular diastole (relaxation). Figure 23 depicts the major divisions of the aorta: the ascending aorta, arch of the aorta, thoracic aorta and abdominal aorta. Major branches of the arch of the aorta, as depicted in Figure 24, are the brachiocephalic trunk (supplying the right upper limb and the right side of the neck and the head), the left common carotid artery (supplying the left side of the neck and the head) and the left subclavian artery (supplying the left upper limb). In the lower abdomen, the abdominal aorta divides into the iliac arteries, which then pass into the legs where they are called

femoral arteries. The femoral arteries and their branches supply the lower limbs. Figure 25 depicts the major arteries in the upper and lower limbs.

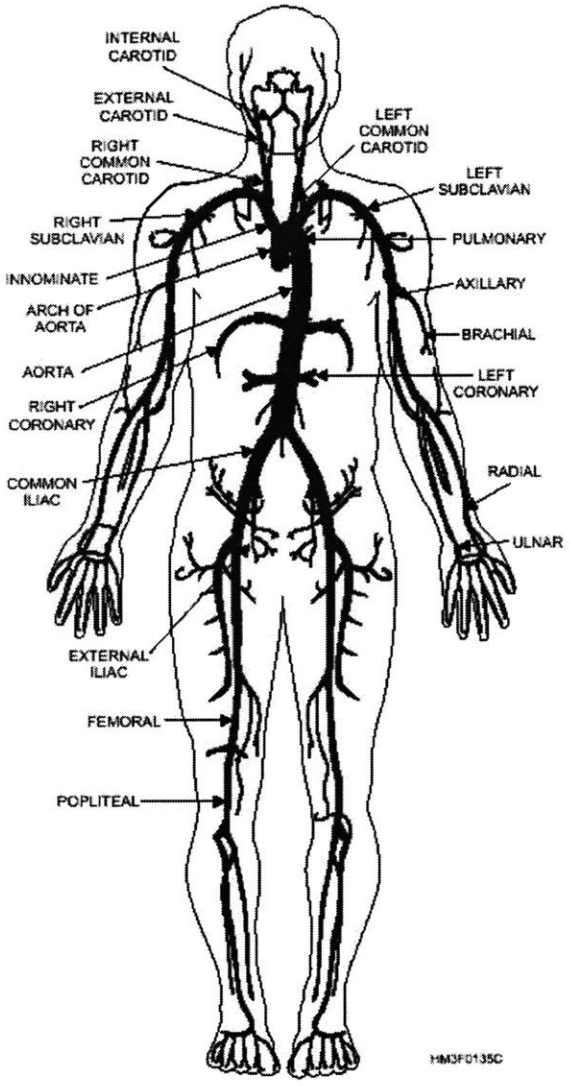

Figure 22. Systemic Arterial Tree [19]

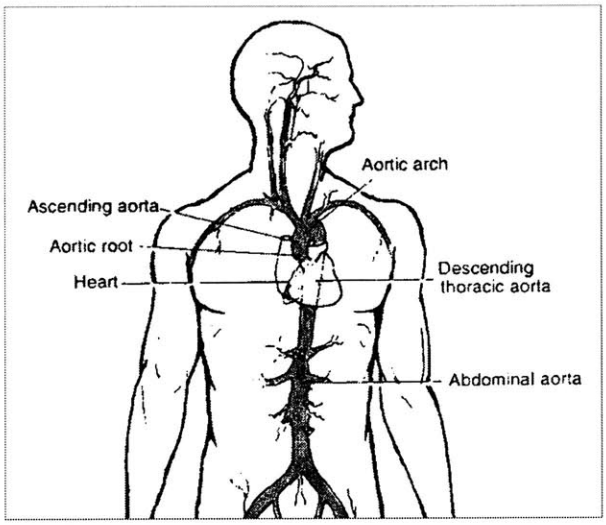

Figure 23. Major Branches of Aorta [20]

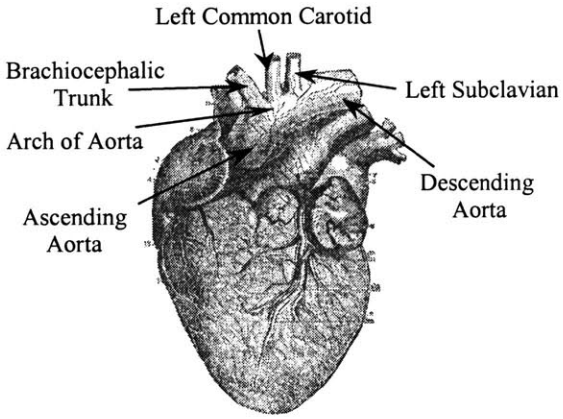

Figure 24. Three Branches of the Arch of Aorta

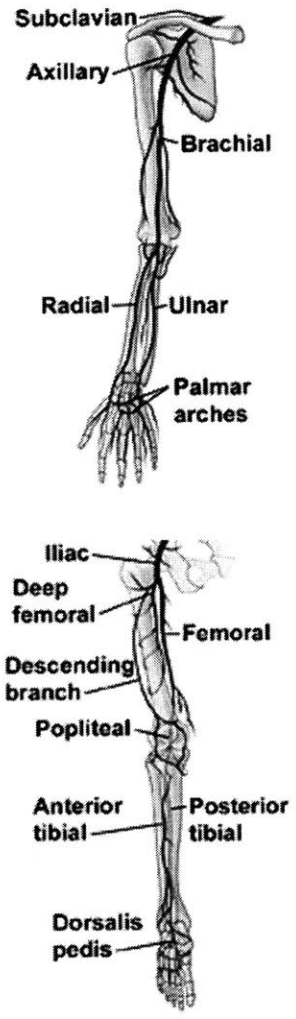

Figure 25. Major Arteries in Upper and Lower Limbs [21]

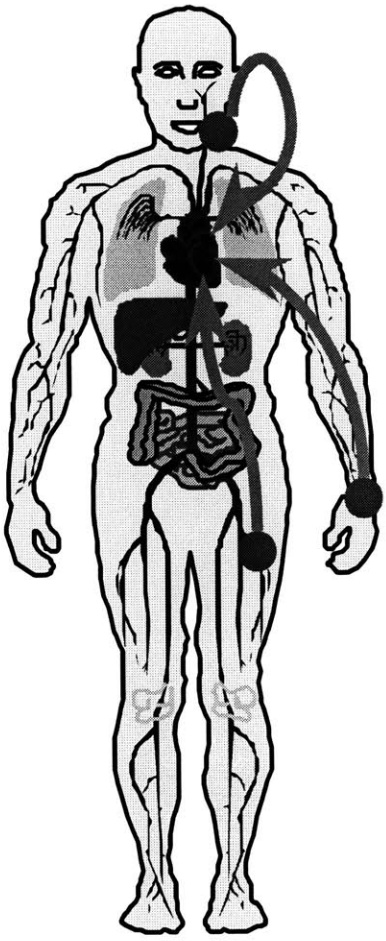

Figure 26. Arterial Multi-channel System

4.1.2 Arterial Multi-channel System

The arterial system has a tree-like structure, topologically similar to the wireless communication system shown in Figure 1. Central hemodynamics are the source that is transmitted distally through different arterial paths. As illustrated in Figure 26, if several sensors are placed at multiple systemic locations, such as the carotid, the radial, the femoral, etc., the central hemodynamics can be observed at multiple peripheral locations. In general, systemic circulation is modeled as a multi-channel system as follows: the left ventricle is modeled as a flow source that is characterized by the aortic flow, the common input to the system; different arterial branches are modeled as the different

channels of the system; multiple sensors, located at different branches of the systemic circulation, are the outputs that are driven by the common input.

4.2 Physiology of Systemic Circulation

4.2.1 Cardiac Cycle

The cardiac events that occur from the beginning of one heartbeat to the beginning of the next are called the cardiac cycle. The cycle consists of a period of cardiac contraction called systole, followed by a period of relaxation called diastole, during which the heart fills with blood. Figure 27 shows the relation between the heart's electrical signals (ECG) and mechanical events (contraction and relaxation) and the consequent changes in central hemodynamics. A brief summary of the cardiac cycle is provided here (refer to Figure 27 for the explanation of different phases). Details of the cardiac cycle can be found in [18][22][23].

The onset of ventricular systole, which is comprised of two phases, coincides with the peak (R) of the QRS complex on an ECG. During the period between the beginning of ventricular contraction and the opening of the semilunar valves, ventricular volume remains constant, thus this phase is called isovolumic contraction. When the left ventricular pressure rises above the aortic pressure (Figure 27), the semilunar valves open and blood begins to pour out of the ventricles (illustrated in Figure 28), which marks the start of the ventricular ejection phase. Near the end of systole, left ventricular pressure falls below aortic pressure, and the forward flowing column of blood in the proximal aorta decelerates and briefly moves retrograde, causing closure of the aortic valve. Once the retrograde flow is resisted by a closed aortic valve, the proximal aortic pressure starts to rise again and the blood in the proximal aorta is once again accellerated in an antegrade direction. This phenomenon produces a bump called the dicrotic notch (i.e.: incisura) on the aortic pressure wave (Figure 27). Ventricular diastole starts with an isovolumic relaxation, during which both the semilunar and the atrioventricular (AV) valves are closed. Major ventricular filling occurs just after the AV valves open (illustrated in Figure 29). Blood that has been flowing into the atria while the ventricles were contracting now rushes into the ventricles. The first third of ventricular filling time thus is known as the period of rapid ventricular filling. During the middle third, called diastasis, a much smaller volume of blood flows into the ventricles. Atrial contraction, i.e., atrial systole, occurs in the last third of the ventricular filling period, which follows the P wave in the ECG and accounts for the small increase in ventricular volume (Figure 27).

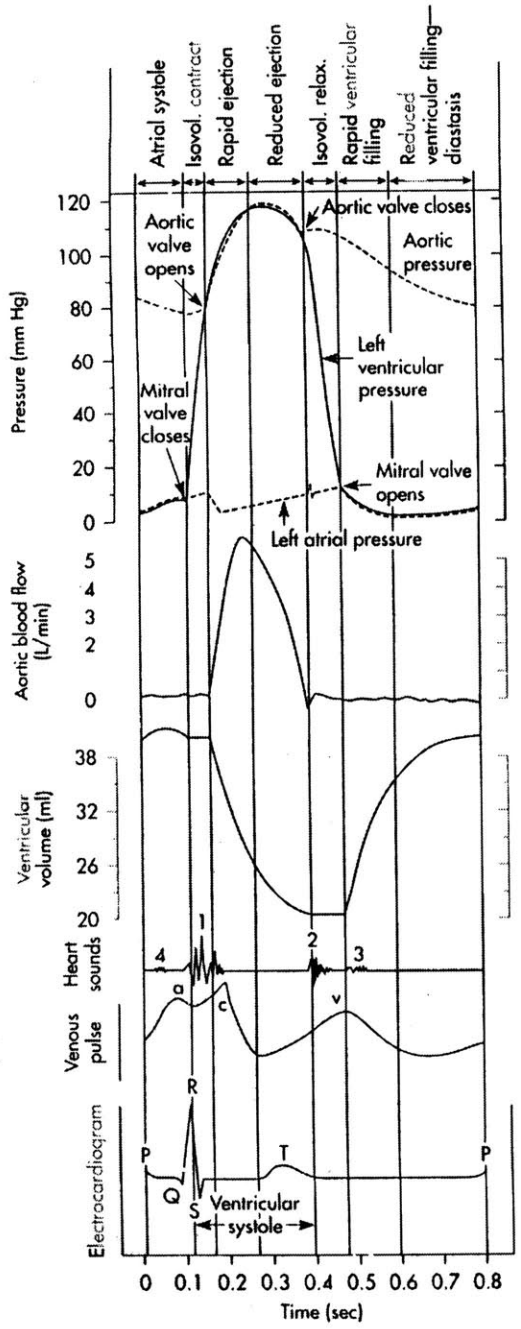

■ Fig. 23-10 Left atrial, aortic, and left ventricular pressure pulses correlated in time with aortic flow, ventricular volume, heart sounds, venous pulse, and the electrocardiogram for a complete cardiac cycle in the dog.

Figure 27. Central Hemodynamics for a Complete Cardiac Cycle [23]

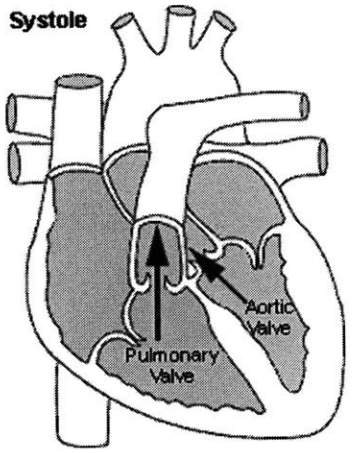

Figure 28. Status of the Valves during Systole

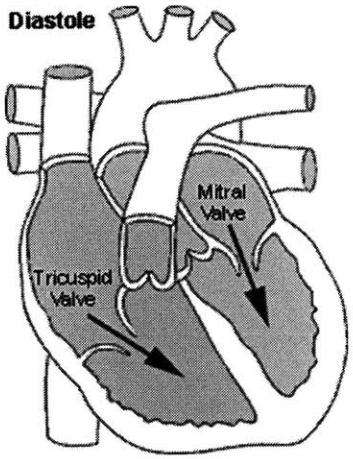

Figure 29. Status of the Valves during Diastole

4.2.2 Determinants of Arterial Blood Pressure

The ejection of blood from the left ventricle during systole generates a pulse wave that can be perceived as arterial blood pressure in peripheral vessels [24]. Arterial blood pressure measured in different arteries is characterized by mean arterial pressure (the area under the arterial pressure curve divided by the cardiac cycle duration), pulse pressure (the amplitude, i.e., the difference between systolic and diastolic pressure) and pulse contour (the waveform). We will discuss the determinants of mean arterial pressure and pulse pressure in this section. Changes in arterial pressure waveform as the pulse wave propagates down the arteries will be discussed in section 4.2.3 . The material of both sections is largely from [23].

The level of the mean arterial pressure depends on two factors: cardiac output and peripheral resistance, as defined in the following equation [18]:

$$\text{Mean Arterial Pressure} = \frac{\text{Cardiac Output}}{\text{Peripheral Resistance}} = \frac{\text{Stroke Volume} \times \text{Heart Rate}}{\text{Peripheral Resistance}} \qquad (115)$$

However, the rate, at which the mean arterial pressure changes, depends on the arterial compliance. The larger the compliance, the slower the mean arterial pressure reaches its steady-state level, as depicted in Figure 30.

The arterial pulse pressure is principally a function of stroke volume and arterial compliance. The left graph in Figure 31 depicts the effect of a change in stroke volume on pulse pressure when heart rate, peripheral resistance and arterial compliance remain the same. An increase in stroke volume results in an increase in mean arterial pressure and an increase in pulse pressure. The right graph in Figure 31 depicts the effect of a change in arterial compliance on pulse pressure when cardiac output and peripheral resistance remain the same. An increase in arterial compliance results in a decrease in pulse pressure.

The determining factors of mean arterial pressure and pulse pressure are summarized in Figure 32. Cardiac output and peripheral resistance determine the average arterial pressure, while stroke volume and arterial compliance determine the amplitude of the arterial pressure.

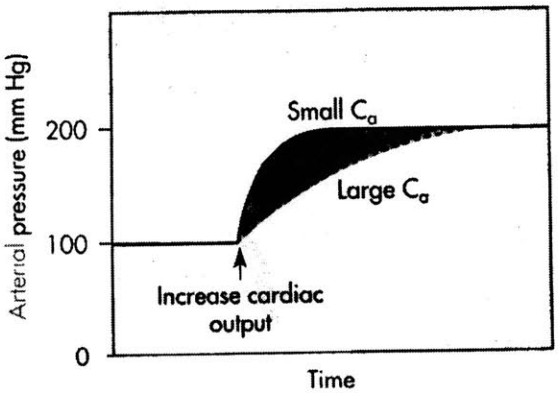

Figure 30. Influence of Cardiac Output and Arterial Compliance on Mean Arterial Pressure [23]

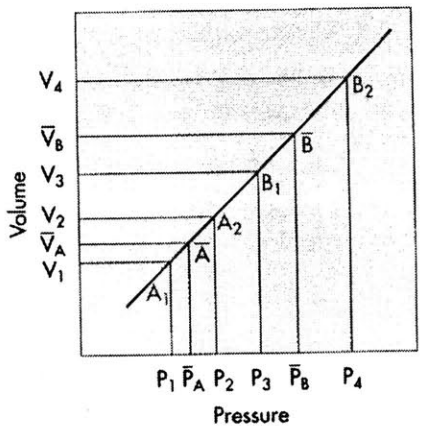

■ **Fig. 26-12** Effect of a change in stroke volume on pulse pressure in a system in which arterial compliance remains constant over the prevailing range of pressures and volumes. A larger volume increment $[(V_4 - V_3) > (V_2 - V_1)]$ results in a greater mean pressure $(\bar{P}_B > \bar{P}_A)$ and a greater pulse pressure $[(P_4 - P_3) > (P_2 - P_1)]$.

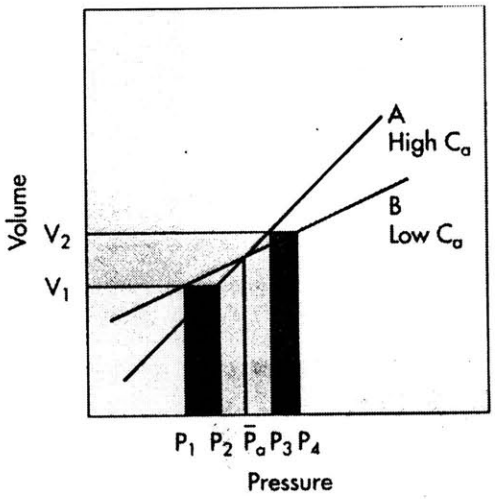

■ **Fig. 26-13** For a given volume increment $(V_2 - V_1)$, a reduced arterial compliance (compliance B < compliance A) results in an increased pulse pressure $[(P_4 - P_1) > (P_3 - P_2)]$.

Figure 31. Influence of Stroke Volume and Arterial Compliance on Pulse Pressure [23]

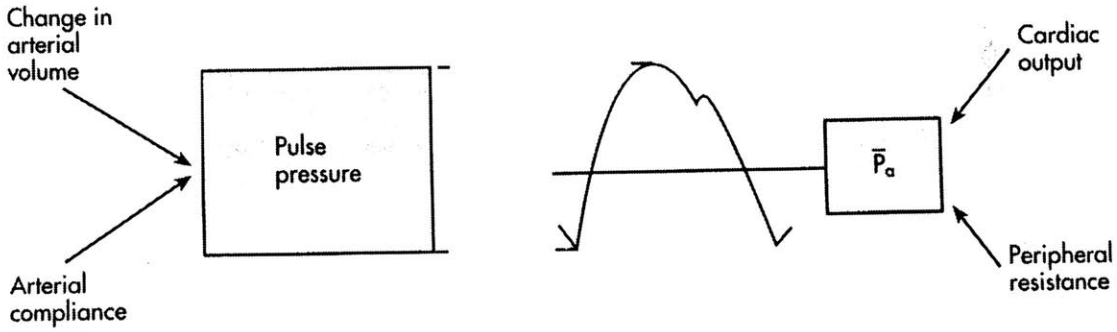

Figure 32. Factors Determining Mean Arterial Pressure and Pulse Pressure [23]

4.2.3 Wave Propagation Along the Arterial Tree

As the pressure wave travels down the arterial tree, the arterial pressure contour becomes distorted. This is demonstrated in Figure 33, which depicts blood pressure waveforms at the proximal aorta, the femoral artery and the radial artery. There are four major changes in the arterial pulse contour as the pressure wave travels distally. First, there is an increasing delay in the onset of the initial pressure rise, which is attributed to the finite pulse wave velocity. In adults, for example, the aortic pulse precedes the brachial artery pulse by about 0.05s [24]. Second, the peripheral pressure wave has a larger pulse pressure (systolic pressure is usually higher and diastolic pressure lower [24]) and has a narrower systolic portion. Figure 34 depicts the arterial pressure curves recorded from various sites in an anesthetized dog. Note that the systolic pressure wave at the knee was 39 mmHg higher than that in the aortic arch and the diastolic pressure was 7 mmHg lower. Third, the high-frequency components of the pulse, such as the incisura, are damped out and soon disappear, largely caused by the viscoelastic properties of the arterial walls. Finally, a hump may appear on the diastolic portion of the pressure wave, in a point in the pressure wave near which the incisura initially appeared. Several factors, including wave reflection, vascular tapering, and pressure-induced changes in transmission velocity, contribute to the peaking of the arterial pressure wave.

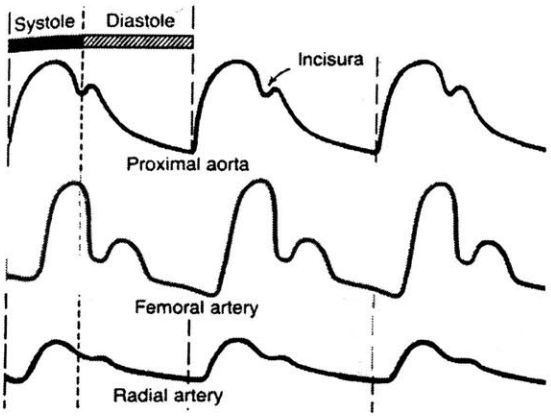

Figure 33. Changes in the Pressure Contour as the Pulse Wave Travels Toward the Periphery [22]

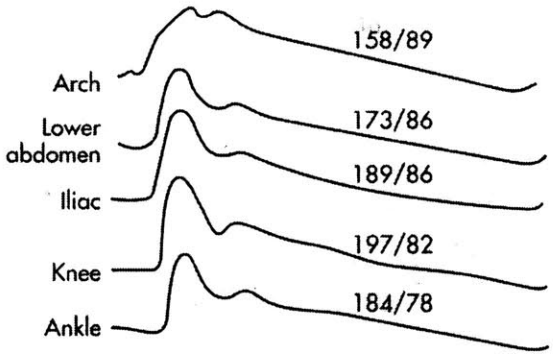

Figure 34. Arterial Pressure Waveforms Recorded at Various Sites along the Arterial Tree in an Anesthetized Dog [23]

4.3 Common and Distinct Dynamics in Systemic Arterial Hemodynamics

The arterial blood pressure waveform measured in the peripheral arteries arises from the interaction between the arterial system and the heart, as illustrated in Figure 35. The characteristics of the heart and the arterial system determine the shape of the arterial pressure waveform. As discussed in section 4.2.2 and 4.2.3 , the major determinants of arterial blood pressure are cardiac output, arterial compliance, peripheral resistance, viscoelasticity, and wave reflection. Cardiac output is a property of the heart, and therefore is modeled as the input to the multi-channel system. Among the other four, arterial compliance and peripheral resistance are common for pressure waves measured at different sites of the arterial system. Viscoelasticity and wave reflection vary with the location of the measurement, thus are different for pressure waves measured at different sites. Table 4 summarizes the corresponding role of each determinant in the multi-channel system.

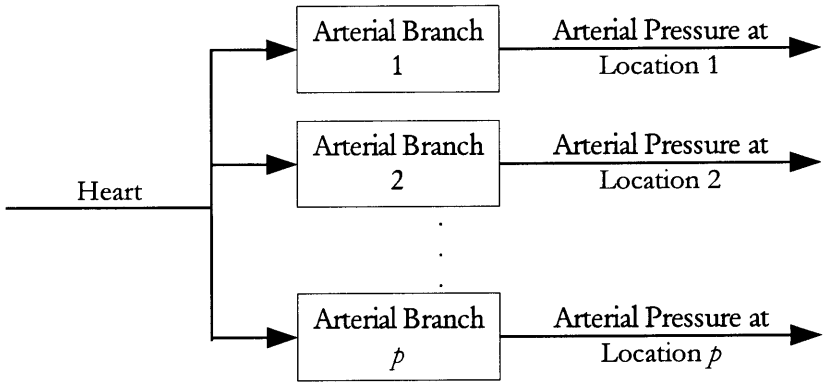

Figure 35. Interaction between Heart and Arterial System

4.3.1 Common Dynamics

Figure 36 depicts how blood pressure changes as the pulse wave travels from the central aorta to the right ventricle. The dashed line is the mean blood pressure. Notice that the mean arterial pressure is almost preserved in the arteries. Therefore, the factors that determine the level of the mean arterial pressure are common for any arterial branches. The common dynamics are thus attributed to the arterial compliance and peripheral resistance, which determine the level of mean arterial pressure and the rate that the mean arterial pressure changes. This models the lumped-parameter nature of

the circulatory system. In fact, the average behavior of the arterial system as a whole can be modeled as a compliance and resistance in parallel, i.e., Windkessel model [25]. The overall time constant of the arterial system is determined by the product of the total arterial compliance and the total peripheral resistance.

Table 4: Determinants of Arterial Blood Pressure

Determinants of Arterial Blood Pressure		Common Factors		Distinct Factors (i.e.: Distinct Dynamics)
		Input	Common Dynamics	
Heart	Cardiac Output	×		
Arterial System	Arterial Compliance		×	
	Peripheral Resistance		×	
	Wave Reflection			×
	Viscoelasticity			×

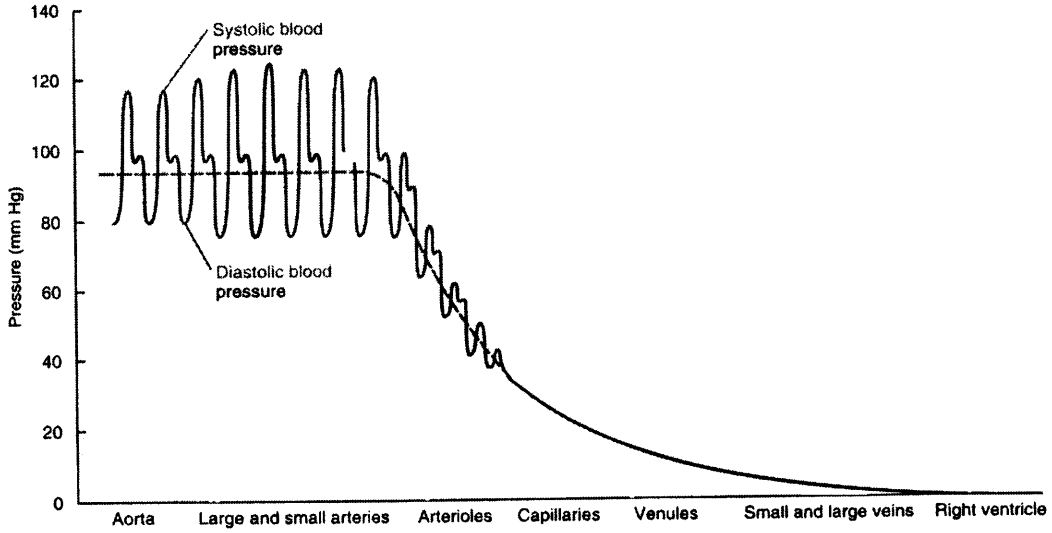

Figure 36. Blood Pressures at Various Locations along the Cardiovascular System [18]

4.3.2 Distinct Dynamics

Recall that Figure 33 and Figure 34 demonstrated the changes in the pressure waveforms at different branches. This feature is attributed to the distinct dynamics of the multi-channel system, which are

attributed to the distributed nature of the circulatory system. The pressure wave, generated by the contraction of the heart, is propagated through the arterial tree. Due to the discontinuity of the caliber or the distensibility in the arterial paths, the wave is reflected back and forth in the channels. Since different paths have different wave propagation characteristics, the dynamics contributed by the wave propagation are distinct for different channels.

4.3.3 Evidence

A 30-element distributed cardiovascular simulator [26][27] is used to study the common dynamics and the distinct dynamics in the arterial system. The simulator generates flow, pressure, velocity, and area signals at different locations of the systemic circulation. Aortic flow is the input to be estimated (cardiac output is the integration of aortic flow over one minute). The branches that are of the greatest interest are the carotid, the brachial, the radial, and the femoral because they can be easily accessed for noninvasive measurements. Figure 37 and Figure 38 depict the simulated aortic blood flow and pressure waveforms at the four previously mentioned locations over one cardiac cycle respectively. Figure 39 plots the impulse responses from the aortic flow to peripheral pressure, i.e., carotid, brachial, femoral and radial pressure, estimated using the standard input-output system identification technique [12]. Obviously the four channels have different initial oscillations, which are dominated by fast-converging, high frequency modes. After the initial oscillations, all of the impulse responses overlap onto the same 'long tail', which is dominated by a slow-converging, low frequency mode. It is clear that all four channels share a common pole. The common dynamics are at low-frequencies and converge slowly, while the distinct dynamics are at high-frequencies and converge quickly.

Similar evidences were observed on the data collected in animal experiments (refer to Chapter 5 for detailed description of the animal study). Figure 40 to Figure 43 plot the impulse responses from the aortic flow to the radial pressure (dashed line) and the femoral pressure (solid line) in four subjects. An interesting finding is that the slope of the tail is different for different subjects. Figure 44 depicts the two impulse responses for two different subjects, which clearly shows that the two subjects have different time constants for the common dynamics.

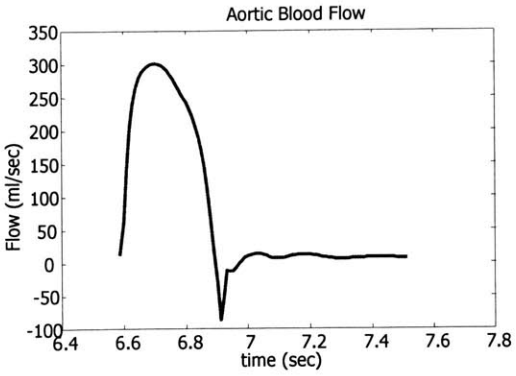

Figure 37. Aortic Flow Generated by the Distributed Cardiovascular Simulator

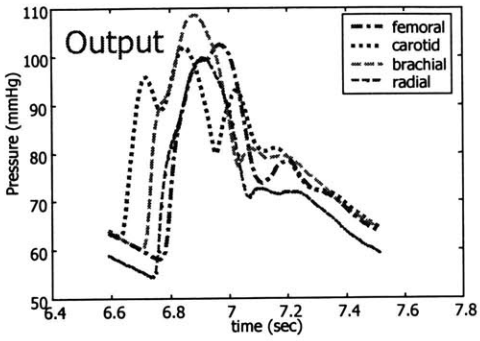

Figure 38. Pressure Signals Generated by the Distributed Cardiovascular Simulator

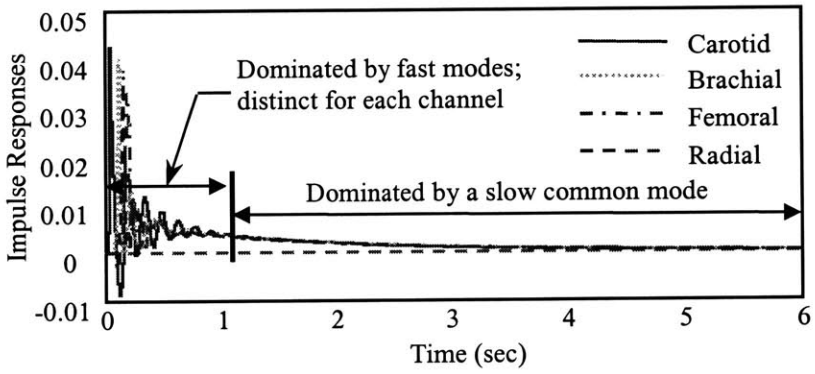

Figure 39. Impulse Responses from Aortic Flow to Peripheral Pressure

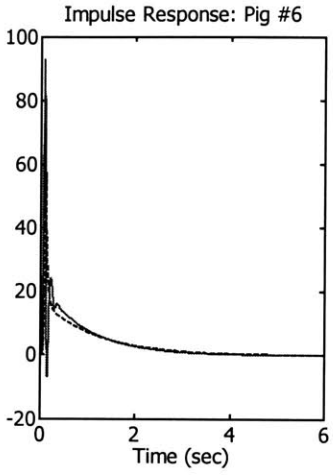

Figure 40. Impulse Responses from Aortic Flow to Radial and Femoral Pressure: Pig # 6

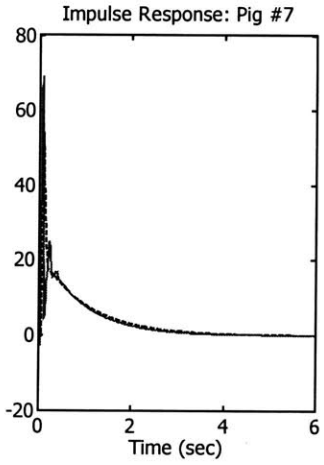

Figure 41. Impulse Responses from Aortic Flow to Radial and Femoral Pressure: Pig # 7

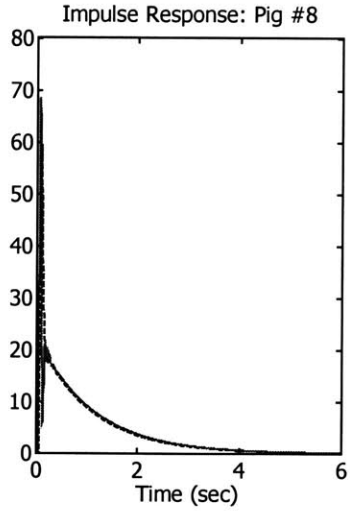

Figure 42. Impulse Responses from Aortic Flow to Radial and Femoral Pressure: Pig # 8

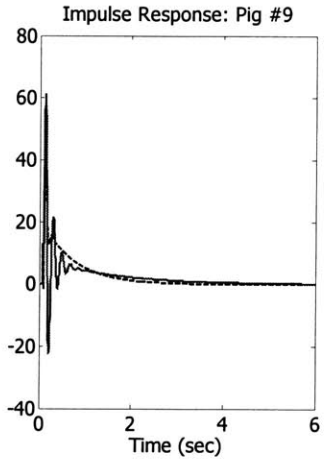

Figure 43. Impulse Responses from Aortic Flow to Radial and Femoral Pressure: Pig # 9

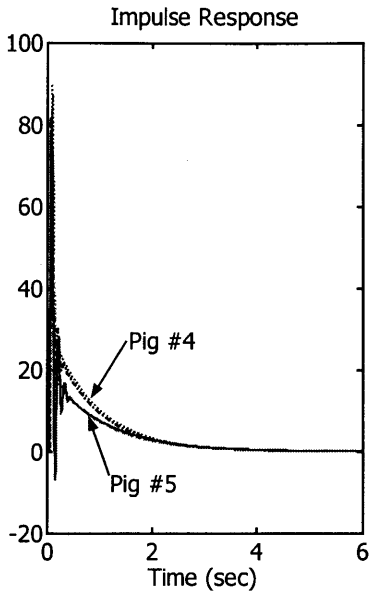

Figure 44. Impulse Responses from Aortic Flow to Radial and Femoral Pressure: Comparison of Pig # 4 and 5

4.4 Identifiability Conditions

4.4.1 Zero-Input Condition

The IIID approach solves the common dynamics by exploiting the zero-input response of the common dynamics, thus requiring the input to be zero for a sufficiently long period. This condition is met for the arterial system due to the intermittent pumping action of the heart: the entire stroke volume is discharged into the systemic circulation during systole, which usually occupies only about one third of the cardiac cycle. Figure 45 illustrates the opening of the aortic semilunar valve during systole and its closure during diastole, which results in the fact that there is no inflow to the systemic circulation during diastole. Revisit Figure 37. The aortic flow, i.e., the input, is almost zero during 60% of a cardiac cycle.

From the discussion in section 4.3, the common dynamics in the systemic arterial hemodynamics only include a common pole, the time constant of which is determined by the total arterial compliance and the total peripheral resistance. The area method [28], which models the arterial system as a Windkessel model, is utilized to estimate the time constant from the diastolic part of the intermediate variable $z(n)$.

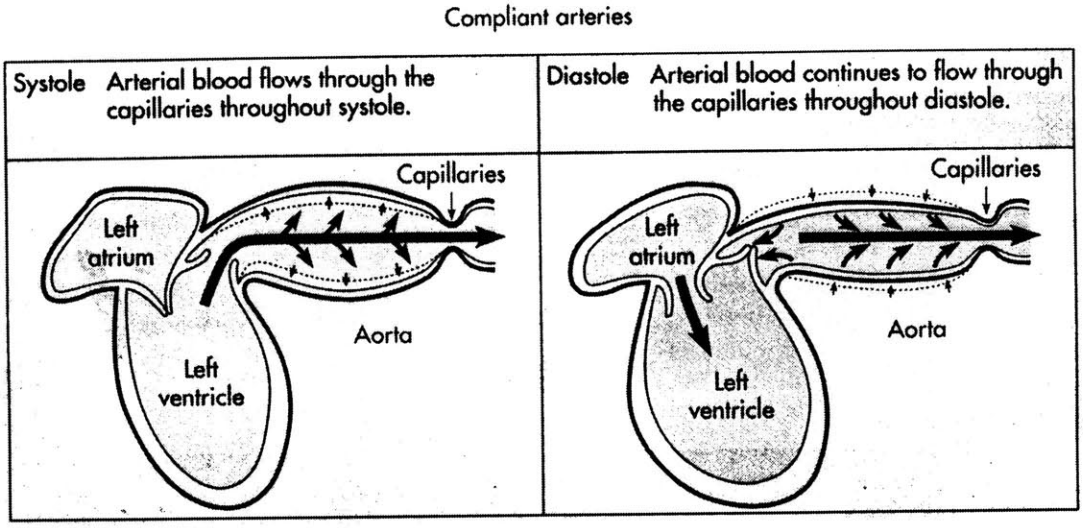

Figure 45. Aortic Semilunar Valve during Systole and Diastole [23]

4.4.2 Input Linear Complexity

Since the aortic flow is almost a periodic signal, the number of modes in the signal, p, is at most T^*F_s [12], where T is the period of one cardiac cycle (s) and F_s is the sampling frequency (Hz). When non-parametric system representation, i.e., finite impulse response, is adopted, it requires that the longest impulse responses of the distinct dynamics of all channels are shorter than $M/(M+1)$ of one cardiac cycle. On the other hand, when parametric system representation, i.e., auto-regressive moving average (ARMA) model, is adopted, the maximum number of parameters needed to characterize one channel should be less than the number of samples in $M/(M+1)$ of cardiac cycle. The number of modes in the input will be higher when considering the beat-to-beat variation induced by respiration and other factors [29]. Apparently, the input-linear-complexity condition is easier to meet when parametric representation is adopted. Therefore, an ARMA model will be adopted in the implementation.

4.5 Numerical Simulations

Numerical simulations were conducted to evaluate the performance of the proposed algorithm. In all the simulations, three channels were used; the channels were modeled by the ARMA representation; the signals were sampled at 100 Hz.

First, the IIID approach was tested on a known three-channel system whose channel dynamics simulate those of the radial, femoral and carotid channels in the cardiovascular simulator.

The pole-zero locations of the three channels are shown (in o) in Figure 46. All the three channels shared a common low-frequency slow-converging mode, which was located at 0.9937. The input signal was the aortic flow generated by the cardiovascular simulator. The outputs were the pressure tracings at the three channels, which are plotted in Figure 47. IIID approach was implemented on the three noise-free outputs. The system order was assumed known. The estimated pole-zero locations of the distinct dynamics of each channel are plotted (in ×) in Figure 46. The intermediate variable was then estimated, from which the common pole was identified. Figure 48 shows the result of the ultimate input estimation – estimated aortic flow compared with the true flow. Obviously, there is a very good matching between the true and estimated flow when the system orders are known and no noise is present.

Second, the IIID approach was tested on the same system while the exact orders of the system were unknown. An upper bound of the channel order was given and the COE algorithm was implemented to estimate the channel order. Figure 49 – Figure 52 show the estimated aortic flow compared with the true flow in four different cases: (a) when the channel order was under-estimated, i.e., the upper bound was smaller than the true channel order; (b), (c), (d) when the channel order was over-estimated by 2%, 4% and 6% respectively. When the channel order was under-estimated, the COE algorithm could not improve the estimation. But when the channel order was over-estimated, the COE algorithm could remove the extraneous roots and over-performed the one without the COE algorithm.

Last, the IIID approach was tested on the pressure signals generated by the cardiovascular simulator. The output signals are plotted in Figure 53. The cardiovascular simulator is distributed and nonlinear, thus the system order was unknown and the channel order estimation algorithm was implemented to estimate the channel orders. Figure 54 shows the estimated aortic flow compared with the true flow.

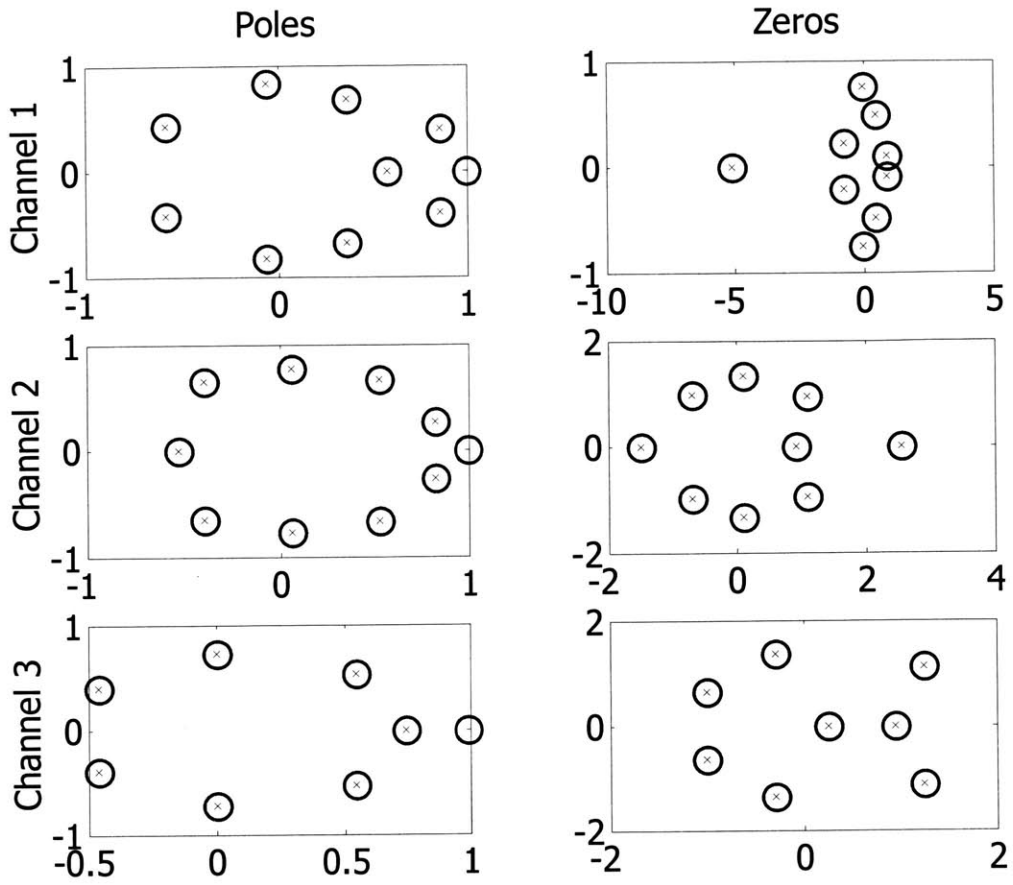

Figure 46. Pole-Zero Location: True vs. Estimated

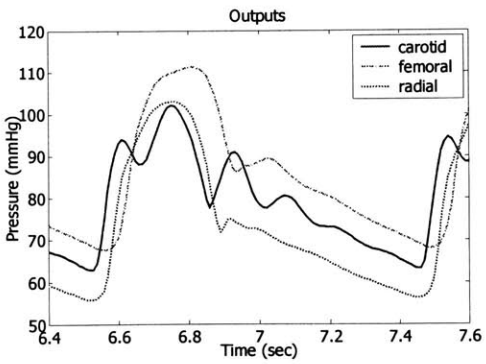

Figure 47. Three Channel Outputs

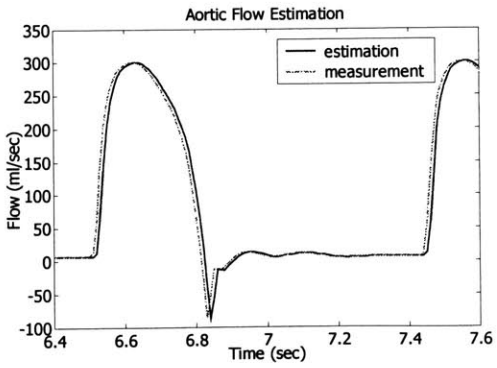

Figure 48. Impulse response estimation when the channel orders are known

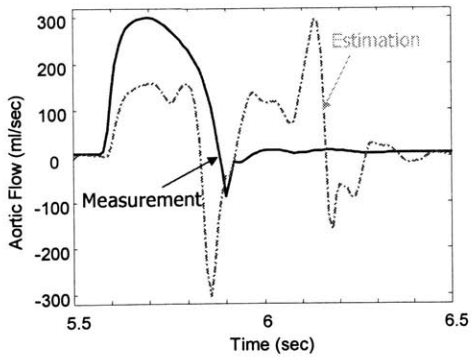

Figure 49. Input Estimation Comparison When Channel Orders are Underestimated

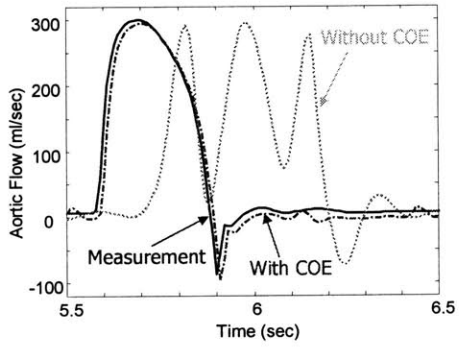

Figure 50. Input Estimation Comparison When Channel Orders are Overestimated by 1

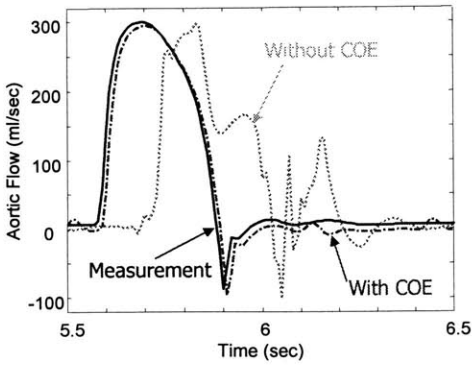

Figure 51. Input Estimation Comparison When Channel Orders are Overestimated by 2

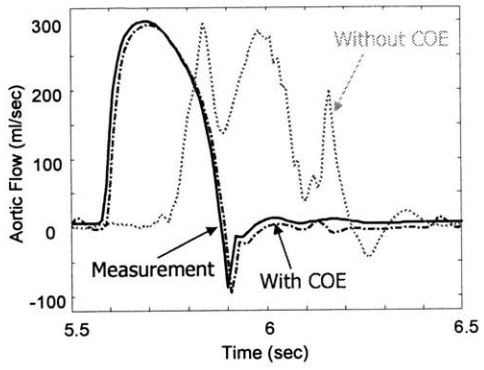

Figure 52. Input Estimation Comparison When Channel Orders are Overestimated by 3

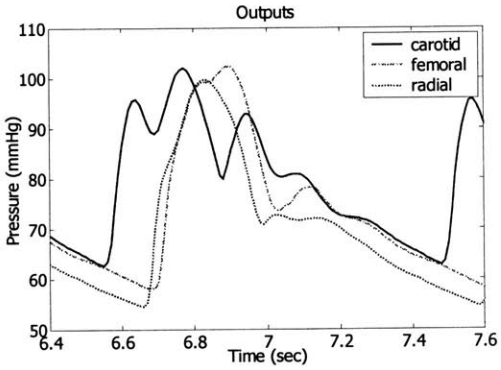

Figure 53. Output Data from the Cardiovascular Simulator

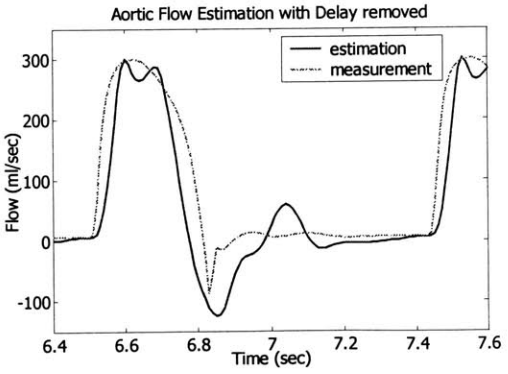

Figure 54. Input Estimation for the Data from the Cardiovascular Simulator

Chapter 5 Animal Experiments

An animal model was explored for validation for the proposed algorithms.

5.1 Animal Preparation

Nine Yorkshire pigs of mass 25 – 35 kg were studied. Swine, a conventional model for cardiovascular investigations, have an arterial tree approximating the human's. The arterial blood pressure waveforms in swine are subject to comparable pressure wave reflections as humans', with the wave reflections being a function of the size and geometry of the arterial tree and the mechanical properties of the vessels.

Prior to experimentation, the animals fasted for 24 hours and were allowed access to water ad libitum. The animals were sedated with intramuscular telazol and zylazine. After orotracheal intubation, the animals were placed on a mechanical ventilator, breathing oxygen, and isoflurane as needed to suppress spontaneous respiration. The swine were maintained at 98 to 101 degrees using Gaymar heating pads and heated crystalloid fluid infusion at a maintenance rate. Via surgical cut-down, a triple lumen central line was placed in the femoral vein, a pair of 7.5 French intravascular introducers placed in the bilateral femoral arteries, and a 22 gauge angiocatheter placed in a distal vessel in the foreleg. Hemostasis was achieved using electrocautery.

A midline sternotomy allowed access to the mediastinum keeping intact one or both pleura. As a gold-standard measurement for cardiac output, a 14 mm Transonic A-series ultrasonic flowprobe was placed around the proximal aorta with generous acoustic couplant. The Millar catheter was advanced through one of the femoral artery introducers to a position in the descending aorta, above the diaphragm. Suprapubic bladder cannulation allowed drainage of urine.

A range of hemodynamic states was studied using cardiovascular drug infusions. The isoflurane tended to reduce total peripheral resistance (TPR), and neosynephrine, a vasoconstricting agent, was infused and weaned to range the blood pressure from approximately 120 mmHg to 60 mmHg. Dobutamine, a positive inotrope and weak vasodilator, was infused (with variable amounts of neosynephrine) to raise the cardiac output to over 5 liters per minute. Esmolol, a beta-one selective antagonist that causes reduced inotropy and chronotropy was infused (with variable amounts of neosynephrine) to reduce cardiac output to less than 1.5 liters per minute. The subjects'

cardiac outputs were lowered to fatal levels using either subsequent hemorrhage or else excess esmolol.

5.2 Instrumentation and Data Acquisition

The following waveforms were collected continuously during the experiments: aortic flow, aortic pressure, femoral pressure, radial pressure, ECG, pulse oximetry, and animal core temperature. Pressure was measured in the central aorta, the left radial and the right femoral artery using Mikro-Tip catheters SPC-350 from Millar Instruments, Inc., which were calibrated in a small cup of water heated to the pig's core temperature. Central aortic flow for comparison purposes was measurement using a Transonic Ultrasonic Probe 14A198 from Transonic Systems Inc. A temperature probe TSD202F from BIOPAC Systems Inc. placed in esophogus continually recorded the core body temperature of the animals. Heart rate and oxygen saturation were monitored by the pulse oximeter TSD123B from BIOPAC Systems, Inc. placed on the chin of the animal. Needle ECG electrodes recorded the electrocardiogram of the animal.

The data pre-filtering, amplification and acquisition were done using the MP150 physiologic data acquisition and analysis system from BIOPAC Systems, Inc. All the signals were sampled at 250 Hz.

5.3 Data Analysis

As discussed in section 3.4, the IIID approach requires the system to satisfy certain identifiability conditions. The input linear complexity condition is one of the most critical requirements on the system. Since ARMA models were used to represent the system, the number of parameters involved in each channel, i.e., the number of poles and zeros, is less than 20. In the animal experiments, the aortic flow measured on the pig is rich in modes due to the beat-to-beat variation naturally presented in the signal; the Hankel matrix always reaches the highest rank as possible. Therefore the input is rich enough to excite all the modes in the system. Another critical requirement is sufficient output samples. Similarly, since parametric representations were adopted, less than one beat of outputs is sufficient, which in turn eases the assumption of a linear, time-variant (LTI) system.

The three channels (aortic, femoral and radial) are modeled using the ARMA representation. The results from one of the pigs are shown from Figure 55 and Figure 61. The three pressure signals are plotted in Figure 55. The COE algorithm was implemented. Figure 56 plots the estimated

intermediate variable. Figure 57 – Figure 59 show the estimated impulse response (solid line) of the aortic, femoral, and radial channel respectively, compared to the estimated impulse responses using standard input-output system identification (dashed line). The comparison of the estimated and the measured aortic flow is shown in Figure 60. Figure 61 shows the linear regression of the two. Figure 62 – Figure 70 show three pressure signals, comparison of the estimated and the measured aortic flow, and the linear regression of the estimation and measurement on another three pigs respectively.

It is noticed from the above result that the IIID estimation of the aortic flow from three pressure tracings captures major features on the measure aortic flow waveform. Some discrepancies exist between the estimation and the measurement, such as the delay between the two. This is partly due to the common delay shared by all the channels. The IIID approach cannot identify the common delay presented in the system since they are common zeros. The delay, however, can be removed using an ECG signal, which will serve as a reference to align the estimation to the real dynamics. Another factor causing the discrepancy is the model limitation. For example, we modeled the channel dynamics as a linear system, although the cardiovascular system is nonlinear. Also, we used a lumped transfer function to describe the channel dynamics, though the real system is distributed and has bi-directional interaction. However, even with these limitations, the IIID approach is still able to capture the major dynamics in the system. Therefore these assumptions are acceptable.

Currently implementation of the IIID approach has certain limitations. Since only two peripheral pressure measurements were taken in the animal experiments, the central aortic pressure was used as the third channel. Although it is acceptable for the purpose of proof-of-principle, central aortic pressure is not easily available in practice. In practical applications, three peripheral pressure measurements at different locations should be taken. The area method currently implemented only uses the signal in the diastole, thus it is difficult to estimate the time constant when the diastole of the cardiac cycle is very short, e.g., when the heart rate is very high. Another system identification technique [30] developed at MIT is expected to solve this issue.

In summary, the positive results from the numerical simulations and initial animal studies demonstrated that the IIID based central hemodynamic monitoring scheme might open the door to noninvasive or minimally invasive cardiovascular monitoring.

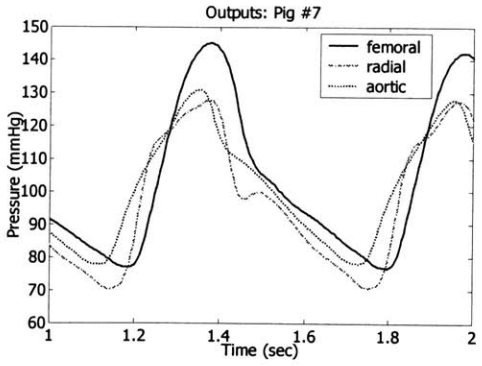

Figure 55. Pressure measurements at Femoral, Radial and Aortic Arteries: Pig # 7

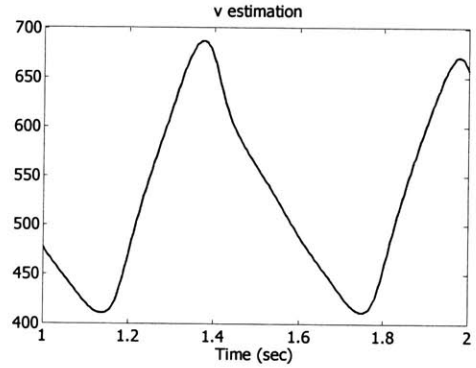

Figure 56. Estimated Intermediate Input: Pig # 7

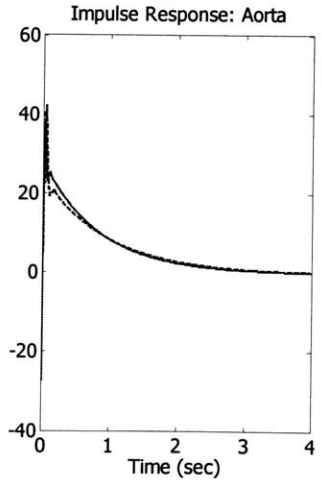

Figure 57. Impulse Response Estimation - Aorta Channel: Pig # 7

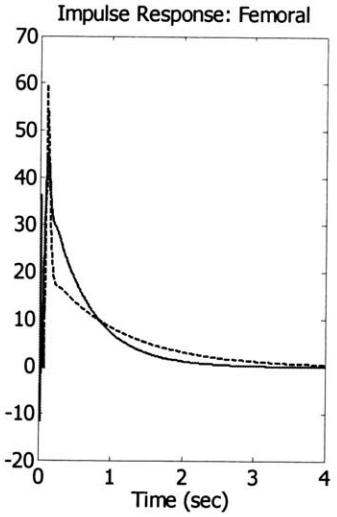

Figure 58. Impulse Response Estimation - Femoral Channel: Pig # 7

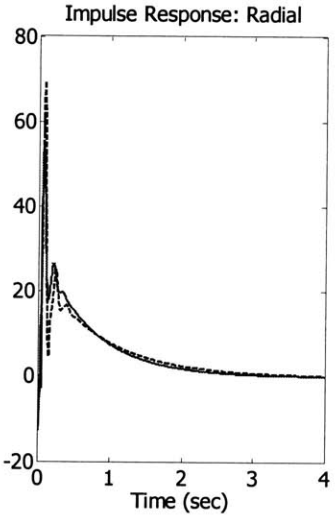

Figure 59. Impulse Response Estimation - Radial Channel: Pig # 7

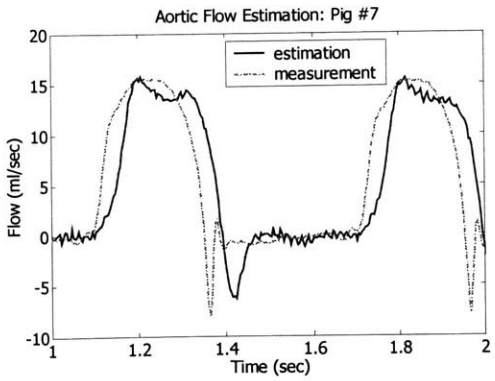

Figure 60. Estimated Aortic Flow Compared with Flowmeter Measurement: Pig # 7

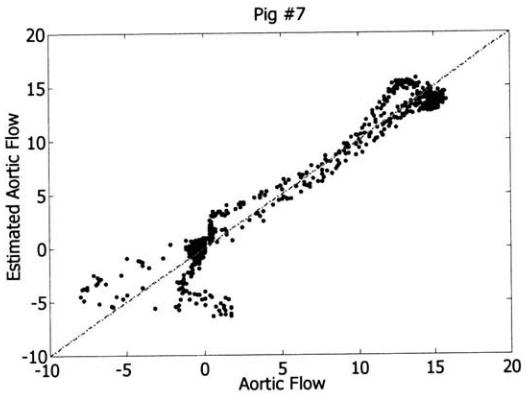

Figure 61. Linear Regression between Estimated and Measured Aortic Flow: Pig # 7

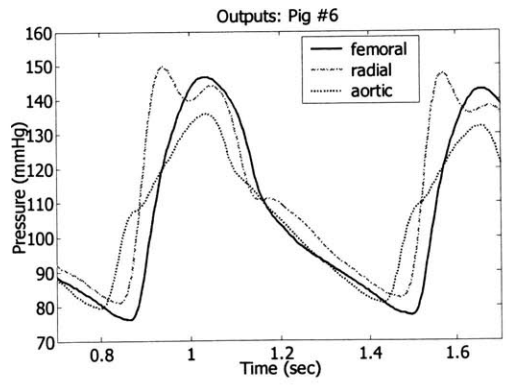

Figure 62. Pressure measurements at Femoral, Radial and Aortic Arteries: Pig # 6

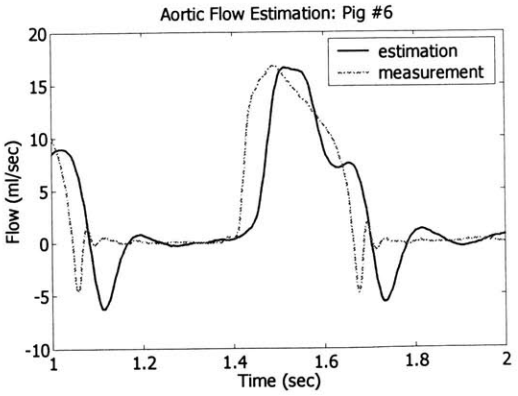

Figure 63. Estimated Aortic Flow Compared with Flowmeter Measurement: Pig # 6

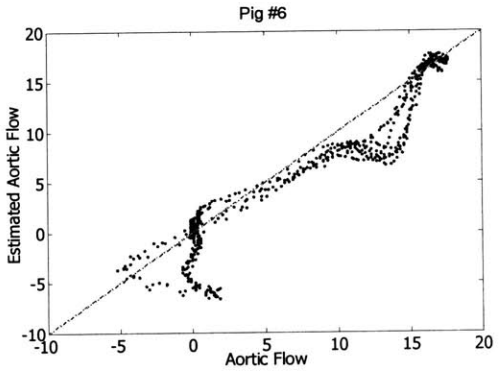

Figure 64. Linear Regression between Estimated and Measured Aortic Flow: Pig # 6

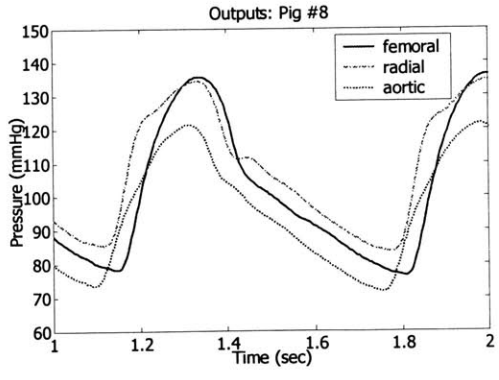

Figure 65. Pressure measurements at Femoral, Radial and Aortic Arteries: Pig # 8

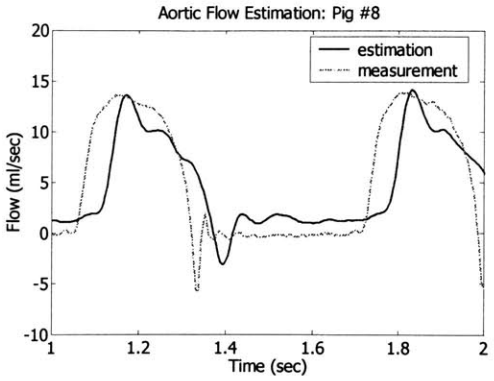

Figure 66. Estimated Aortic Flow Compared with Flowmeter Measurement: Pig # 8

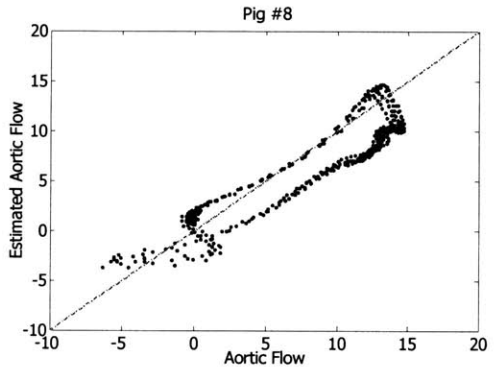

Figure 67. Linear Regression between Estimated and Measured Aortic Flow: Pig # 8

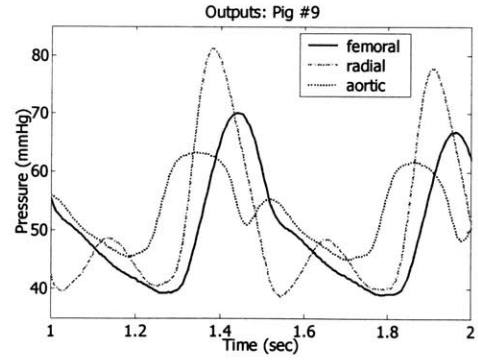

Figure 68. Pressure measurements at Femoral, Radial and Aortic Arteries: Pig # 9

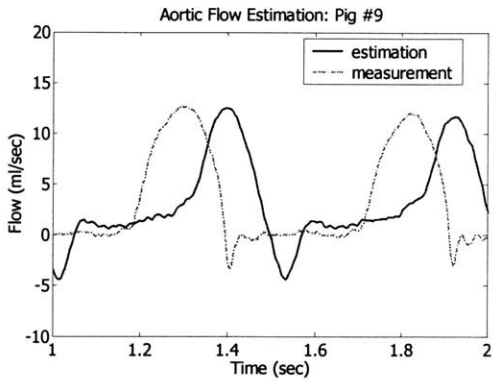

Figure 69. Estimated Aortic Flow Compared with Flowmeter Measurement: Pig # 9

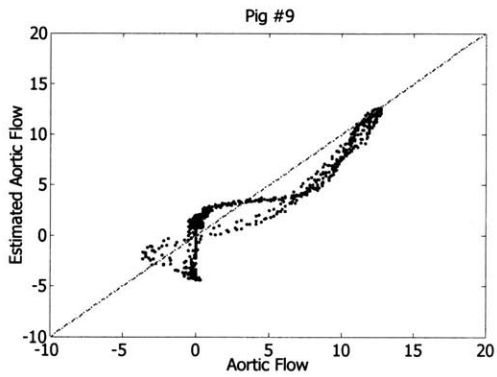

Figure 70. Linear Regression between Estimated and Measured Aortic Flow: Pig # 9

Chapter 6 Conclusions

6.1 Summary of Contributions

This thesis develops the IIID approach for multi-channel blind system identification when common dynamics are present and applies it to central hemodynamic monitoring.

- The MBSI research is thoroughly surveyed. The proof of the sufficient and necessary conditions is extended for systems that have IIR. MBSI is difficult when common dynamics are present in the multi-channel system because the modes in the input as well as the common dynamics are common for all the channels. Given only the outputs, existing MBSI algorithms cannot distinguish between the input and the common dynamics. This is a problem that has not been tackled by previous research, although it is very common in practice, especially for the systems that have both a lumped-parameter nature and a distributed nature, such as the cardiovascular system.
- A new interpretation of the MBSI problem when common dynamics are proposed and the IIID approach is developed to solve the problem. IIID approach treats the common factors in the system, i.e., the input and the common dynamics in all channels, as the input to a new multi-channel system, and therefore solves the distinct dynamics by identifying the new multi-channel system. The zero-input response is then exploited to solve for the common dynamics, which requires that the input to the system be zero for a sufficiently long period.
- The sufficient and necessary conditions for the distinct dynamics identification are derived. A series of theorems describes the input-linear-complexity condition and gives the solution to the distinct dynamics identification. In particular, the relationship between the linear-complexity condition of the original input and that of the intermediate input is given; the case when the channel orders are overestimated is investigated thoroughly.
- This thesis discovers the similarity between the structure of the digital wireless communication system and that of the cardiovascular system and is the first to model the systemic circulation as a multi-channel system and to propose the cardiovascular MBSI for central hemodynamic monitoring. The input, the common dynamics and the distinct

dynamics in the cardiovascular multi-channel system are explained based on the explanation of the determinants of the arterial blood pressure.

- The proposed central hemodynamic monitoring technique is tested on a cardiovascular simulator and on data taken from pigs. Results from the standard input-output system identification on the data from the simulator or from the animal experiments verify the explanation for the common dynamics and distinct dynamics. Results from the multi-channel blind system identification verify that the IIID approach could open up the possibility of noninvasive central hemodynamic monitoring, which reduces the risks that might be exposed to the patients.

6.2 Future Directions for Research

There are several potential areas of future research that could expand upon the work in this thesis.

First, additional animal studies with three peripheral pressure measurements would be needed to further validate the utility of this method in central hemodynamic monitoring. The current implementation of the IIID approach estimates the aortic flow within a scalar factor. Whether and how the scalar factor could be reserved for several runs of MBSI is critical when continuous monitoring of aortic flow is demanded.

Second, according to [24], as the heart beats faster, the relaxation period (diastole) becomes shorter and shorter whereas the duration of the contraction period (systole) shortens only slightly. The area method currently implemented for common dynamics identification only uses the signal in the diastole, thus it is difficult to estimate the time constant when the diastole of the cardiac cycle is very short, e.g., when the heart rate is very high. It would be interesting to see how the IIID approach could be integrated with another method [30] developed at MIT for the estimation of the time constant.

Third, the channel dynamics from the central aortic flow to the peripheral pressure are expected to be different under different diseases. It is demonstrated in distinctive changes observed in the pressure waveforms under different condition of the circulation. Figure 71 depicts the pressure pulse contours in arteriosclerosis, aortic stenosis, patent ductus arteriosus and aortic regurgitation. More interestingly, the pressure pulse contour could be different even when the aortic flow does not change much. Figure 72 depicts the pressure waveforms generated in a normal subject (upper left curve) and a hypertensive subject (upper right curve), even when both have the same

ventricular ejection curve (lower curves) [31]. This suggests that the identification of the channel dynamics could be of clinical value.

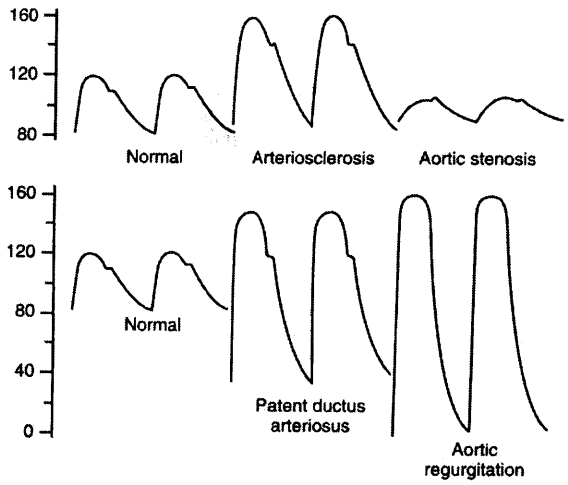

Figure 71. Arterial Pressure Contour Changes in Different Diseases [22]

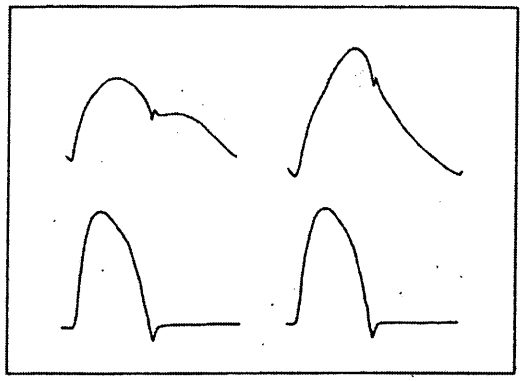

Fig 1.—Diagrammatic representation of ascending aortic flow wave (lower waves) and pressure wave (upper waves) in subject with high arterial compliance, at left, and in subject whose arterial compliance is reduced by hypertension and arterial degeneration, at right.

Figure 72. Aortic Flow and Pressure in Normal and Hypertensive Subject [31]

Appendix A. Proof of *Theorem 1* for All-zero Systems

Proof:

(*Necessity*) If $p < L$, it can be shown that the channels are not uniquely identifiable even if the input $u(n)$ is known. Since blind system identification does not have any knowledge of $u(n)$, the necessary condition of standard system identification should also be that of blind system identification.

With the known input, the identification of the channel impulse responses can be found be solving

$$\begin{bmatrix} y_i(L) \\ \vdots \\ y_i(N) \end{bmatrix} \equiv \begin{bmatrix} u(1) & \cdots & u(L) \\ \vdots & \ddots & \vdots \\ u(N-L+1) & \cdots & u(N) \end{bmatrix} \begin{bmatrix} h_i(L) \\ \vdots \\ h_i(1) \end{bmatrix} \tag{116}$$

Since $p < L$, the input Hankel matrix in eq. (116) is rank deficient. Clearly, eq. (116) does not have a unique solution. Therefore, it requires L or more modes to achieve blind system identification.

(*Sufficiency*)

For a two-channel all-zero system, the channel outputs also satisfy eq.(30), except that $L = L_h$ in this case. Therefore eq. (31) – eq. (33) become:

$$\mathbf{U}(L) \equiv \begin{bmatrix} u(1) & \cdots & u(2L-1) \\ \vdots & \ddots & \vdots \\ u(N-2L+2) & \cdots & u(N) \end{bmatrix} : \{(N-2L+2) \times (2L-1)\} \tag{117}$$

$$\mathbf{H}(L) \equiv [\mathbf{H}_2(L), \quad -\mathbf{H}_1(L)] : \{(2L-1) \times 2L\} \tag{118}$$

$$\mathbf{H}_i(L) \equiv \begin{bmatrix} h_i(L) & & \\ \vdots & \ddots & \\ h_i(1) & \cdots & h_i(L) \\ & \ddots & \vdots \\ & & h_i(1) \end{bmatrix} : \{(2L-1) \times L\}, i = 1, 2 \tag{119}$$

$p \geq 2L\text{-}1$ implies that $\mathbf{U}(L)$ has full column rank. Therefore the null space of the matrix $\mathbf{Y}(L)$ is the same as the null space of the matrix $\mathbf{H}(L)$. Since $\mathbf{H}(L)$ has a column rank of $2L$-1, the MBSI problem has a unique solution.

End of Proof.

Appendix B. Nomenclature

General MBSI Formulation	
$u(n)$	Input to the multi-channel system
$U(z^{-1})$	z-transform of $u(n)$
M	Number of channels in the multi-channel system
$y_i(n), i = 1,...,M$	Output of channel i
$Y_i(z^{-1}), i = 1,...,M$	z-transform of $y_i(n), i = 1,...,M$
$h_i(n), i = 1,...,M$	Impulse response of channel i
$H_i(z^{-1}), i = 1,...,M$	Transfer function of channel i, i.e., z-transform of $h_i(n), i = 1,...,M$
$N_i(z^{-1}), i = 1,...,M$	Numerator of the transfer function $H_i(z^{-1}), i = 1,...,M$
$m_i, i = 1,...,M$	Order of the polynomial $N_i(z^{-1}), i = 1,...,M$
$b_{i,k}, k = 0,...,m_i, i = 1,...,M$	Coefficients of the polynomial $N_i(z^{-1}), i = 1,...,M$
$D_i(z^{-1}), i = 1,...,M$	Denominator of the transfer function $H_i(z^{-1}), i = 1,...,M$
$n_i, i = 1,...,M$	Order of the polynomial $D_i(z^{-1}), i = 1,...,M$
$a_{i,k}, k = 0,...,n_i, i = 1,...,M$	Coefficients of the polynomial $D_i(z^{-1}), i = 1,...,M$
$L_i, i = 1,...,M$	Length of the impulse response $h_i(n)$ if it has finite length
L_h	Approximated length of the impulse response $h_i(n)$ if it has infinite length
L	Maximum order of all the channels
N	Number of input samples available
$\mathbf{Y}_i, i = 1,...,M$	Output Hankel matrix of channel i
$\mathbf{Y}$	Output matrix of all M channels
$\mathbf{h}_i, i = 1,...,M$	Impulse response vector of channel i
$\mathbf{h}$	Impulse response vector of all M channels
$\mathbf{D}_i, i = 1,...,M$	Denominator vector of channel i
$\mathbf{D}$	Denominator vector of all M channels
$\mathbf{N}_i, i = 1,...,M$	Numerator vector of channel i
$\mathbf{N}$	Numerator vector of all M channels
$\mathbf{W}_i, i = 1,2$	General vector of the MBSI problem
$W_i(z^{-1}), i = 1,2$	Polynomial with coefficients defined in $\mathbf{W}_i, i = 1,2$
$\mathbf{Y}(L)$	General form of output Hankel matrix
$\mathbf{Y}_i(L), i = 1,2$	General form of output Hankel matrix of channel i
$\mathbf{H}(L)$	General form of impulse response Hankel matrix
$\mathbf{H}_i(L), i = 1,2$	General form of impulse response Hankel matrix of channel i
$\mathbf{U}(L)$	General form of input Hankel matrix

New MBSI Formulation when Common Dynamics are Present	
$h_i'(n), i = 1,...,M$	Impulse response of the distinct dynamics of channel i
$\mathbf{h}_i', i = 1,...,M$	Impulse response vector of the distinct dynamics of channel i
$H_i'(z^{-1}), i = 1,...,M$	Transfer function of the distinct dynamics of channel i, i.e., z-transform of $h_i'(n)$
$N_i'(z^{-1}), i = 1,...,M$	Numerator of the transfer function $H_i'(z^{-1}), i = 1,...,M$
$m_i', i = 1,...,M$	Order of the polynomial $N_i'(z^{-1}), i = 1,...,M$
$b_{i,k}', k = 0,...,m_i', i = 1,...,M$	Coefficients of the polynomial $N_i'(z^{-1}), i = 1,...,M$
$D_i'(z^{-1}), i = 1,...,M$	Denominator of the transfer function $H_i'(z^{-1}), i = 1,...,M$
$n_i', i = 1,...,M$	Order of the polynomial $D_i'(z^{-1}), i = 1,...,M$
$a_{i,k}', k = 0,...,n_i', i = 1,...,M$	Coefficients of the polynomial $D_i'(z^{-1}), i = 1,...,M$
$h_0(n)$	Impulse response of the common dynamics of all the channels
$H_0(z^{-1})$	Transfer function of the distinct dynamics of all the channels, i.e., z-transform of $h_0(n)$
$N_0(z^{-1})$	Numerator of the transfer function $H_0(z^{-1})$
m_0	Order of the polynomial $N_0(z^{-1})$
$b_{0,k}, k = 0,...,m_0$	Coefficients of the polynomial $N_0(z^{-1})$
$D_0(z^{-1})$	Denominator of the transfer function $H_0(z^{-1})$
n_0	Order of the polynomial $D_0(z^{-1})$
$a_{0,k}, k = 0,...,n_0$	Coefficients of the polynomial $D_0(z^{-1})$
$v(n)$	Intermediate input to the multi-channel system
$V(z^{-1})$	z-transform of $v(n)$
L_c	Order of the common dynamics
L_d	Maximum order of the distinct dynamics of all the channels
ΔK	Difference between the orders of the distinct dynamics of the two channels
L_e	Estimated maximum order of the distinct dynamics of all the channels
K	Number by that the maximum order of the distinct dynamics is overestimated
$\mathbf{Y}_i(L_d), i = 1,2$	Output Hankel matrix of channel i when exact order of the channel is known
$\mathbf{Y}(L_d)$	Output matrix of all channels when exact order of the channel is known
$\mathbf{H}_i'(L_d), i = 1,2$	Impulse response Hankel matrix of the distinct dynamics of channel i when exact order of the channel is known
$\mathbf{V}(L_d)$	Intermediate input Hankel matrix when exact order of the channel is known

$\mathbf{H}_0(L_d)$	Impulse response Hankel matrix of the common dynamics when exact order of the channel is known
$\mathbf{U}(L_d)$	Input Hankel matrix when exact order of the channel is known
$\mathbf{Y}_i(L_e), i = 1,2$	Output Hankel matrix of channel i when channel order is overestimated
$\mathbf{Y}(L_e)$	Output matrix of all channels when channel order is overestimated
$\mathbf{H}_i'(L_e), i = 1,2$	Impulse response Hankel matrix of the distinct dynamics of channel i when channel order is overestimated
$\mathbf{V}(L_e)$	Intermediate input Hankel matrix when channel order is overestimated
$\mathbf{H}_0(L_e)$	Impulse response Hankel matrix of the common dynamics when channel order is overestimated
$\mathbf{U}(L_e)$	Input Hankel matrix when channel order is overestimated
α	An arbitrary constant
$\theta_{\Delta K}(z^{-1})$	Polynomial of order ΔK whose roots are at the origin
$\theta_1(z^{-1})$	Polynomial of order K whose roots are at arbitrary locations
$\theta_2(z^{-1})$	polynomial of order K whose roots are at arbitrary locations
$\Omega\{\bullet\}$	Roots of a polynomial
$\square\{\bullet\}$	Null space of a matrix
p	Number of modes in a finite sequence
p_u	Number of modes in $u(n)$
p_v	Number of modes in $v(n)$
$\mathbf{U}(p)$	p^{th}-order Hankel matrix of sequence $u(n)$
$R_u(n)$	auto-correlation of the sequence $u(n)$
$\mathbf{R}(p)$	p^{th}-order Toeplitz matrix of the auto-correlation of the sequence $u(n)$

Appendix C. Cardiovascular Simulator

The signals used in the numerical simulation in this thesis are generated by a 30-element distributed cardiovascular simulator, which was originally developed by Dr. E. T. Ozawa [26], and was further refined by Karen E. Bottom and Xinshu Xiao [27] at MIT. This simulator is based upon a numerical solution of the one-dimensional equations of motion in a geometrically accurate branching network of the arterial system, including energy losses at bifurcations, a ventricular model incorporating specified time-dependent wall compliances and unidirectional valves, and lumped-parameter venous and pulmonary circulatory systems. Also incorporated are damping mechanisms related to the phase dependence of the wall shear during periodic flows and the viscoelastic behavior of the arterial walls. The simulator is capable of reproducing flow, pressure, velocity, and area signals at different locations of the systemic circulation. Figure 73 shows the schematic of the model. Dashed elements represent those that are reflected by symmetry and are not explicitly computed.

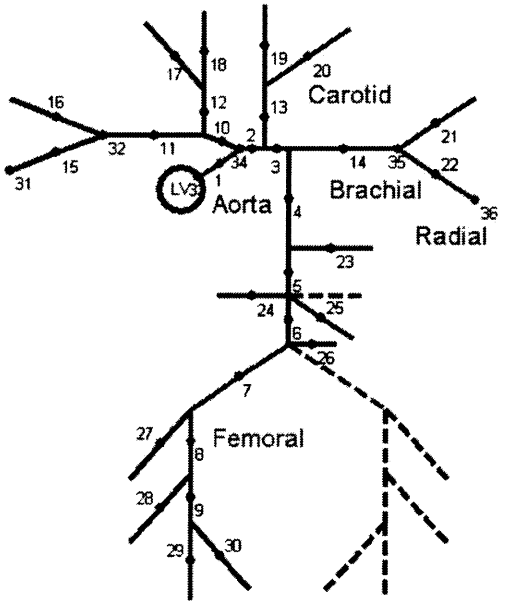

Figure 73. Schematic of the Distributed Arterial Model

Appendix D. Protocol Approval from MIT

MASSACHUSETTS INSTITUTE OF TECHNOLOGY
COMMITTEE ON ANIMAL CARE
BLDG. 16-408
CAMBRIDGE, MA 02139
tel. 617 253-9436/fax 617 258-8257
NOTICE OF COMMITTEE REVIEW

Date: November 5, 2001
Proposal #: 01-055
Proposal Title: Multi-channel Blind System Identification for Noninvasive Cardiovascular Monitoring
Principal Investigator: Harry Asada/Andrew Reisner Department: MEC
Funding Agency: Harvard/MIT Center for Integration of Medicine and Innovative Technology (CIMIT)
Grant #: pending

x New Proposal ___ Three-year Renewal _____ Annual Renewal
_____ Addendum ___ Teaching Proposal ___ Expedited Review

The above-named proposal was reviewed at the November 1, 2001 meeting of the Committee on Animal Care. This is to inform you of the following:

x Approval*

_____ Approval with the provisions listed below.

_____ Approval limited to ____ days, pending receipt of the additional information requested below.

___ Approval deferred pending receipt of information requested below.

___ Disapproved for the reasons described below.

The following provisions and/or suggestions have been made by the CAC:

Reasons for disapproval:

*Projects involving the use of biohazardous material (radioisotopes, infectious agents, carcinogens, as examples) require separate approval by the Radiation Protection Office, Industrial Hygiene Office/ Environmental Medical Service, or the Biosafety Office. The Committee on Animal Care approval is contingent on the approval of these separate MIT committees. Animal work should not commence until all approvals have been received by the Principal Investigator.

This institution has an Animal Welfare Assurance on file with the Office for Laboratory Animal Welfare. The Assurance number is A-3125-01.

Action described in this notice applies for 12 months from the date of approval or the time indicated and is based on the assumption that no substantive changes in experimental procedures dealing with animals used will occur during the period unless approval for the revised procedure(s) is obtained from the Committee on Animal Care.

Chair, CAC

Assoc. Dir, Office of Sponsored Programs/Grants Management

References

[1] C. Hori, *et al.*, "Estimation of aortic BP waveform from noninvasive radial tonometry; validation of FFT and ARX methods," *Proceedings of the 19th Annual International Conference of the IEEE EMBS*, Vol. 3, pp. 1142 - 1145, 1997.

[2] B. Fetics, *et al.*, "Parametric model derivation of transfer function for noninvasive estimation of aortic pressure by radial tonometry," *IEEE Transactions on Biomedical Engineering*, 46(6), pp. 698 - 706, 1999.

[3] Abed-Meraim, *et al.*, "Blind system identification," *Proceedings of the IEEE*, 85(12), pp. 1310 - 1332, 1997.

[4] L. Tong, *et al.*, "Blind identification and equalization based on second-order statistics: a time domain approach," *IEEE Transactions on Signal Processing*, 40(2), pp. 340 - 349, 1994.

[5] W. A. Gardner, "A new method of channel identification," *IEEE Transactions on Communication*, 39(6), pp. 813 - 817, 1991.

[6] G. Xu, *et al.*, "A Least-squares approach to blind channel identification," *IEEE Transactions on Signal Processing*, 43(12), pp. 2982 - 2993, 1995.

[7] H. Liu, *et al.*, "Recent development in blind channel equalization: from cyclostationarity to subspaces," *Signal Processing*, Vol. 50, pp. 83 - 99, 1996.

[8] L. Tong and S. Perreau, "Multichannel blind identification: from subspace to maximum likelihood methods," *Proceedings of the IEEE*, 86(10), pp. 1951 - 1968, 1998.

[9] M. I. Gurelli and C. L. Nikias, "EVAM: an eigenvector-based algorithm for multichannel blind deconvolution of input colored signals," *IEEE Transactions on Signal Processing*, 43(1), pp. 134 - 149, 1995.

[10] H. Liu, G. Xu, and L. Tong, "A deterministic approach to blind equalization," Conference Record of The Twenty-Seventh Asilomar Conference on Signals, Systems and Computers, Vol. 1, pp. 751 - 755, 1993.

[11] T. K. Moon and W. C. Stirling, *Mathematical Methods and Algorithms for Signal Processing*, Prentice Hall, Upper Saddle River, NJ, 2000.

[12] L. Ljung, *System Identification*, Prentice Hall, Upper Saddle River, NJ, 1999.

[13] Y. Zhang, H. H. Asada and A. T. Reisner, "Noninvasive cardiac output monitoring based on multi-channel blind system identification and model decomposition," 2002 IEEE EMBS and BMES conference, accepted.

[14] A. G. Hamilton, *Linear Algebra: An Introduction with Concurrent Examples*, Cambridge University Press, Cambridge, England, 1989.

[15] M. Wax and T. Kailath, "Detection of signals by information theoretic criteria," IEEE Transactions on ASSP, 33(2), pp. 387 - 392, 1985.

[16] J.-J. Fuchs, "Estimating the number of sinusoids in additive white noise," IEEE Transactions on ASSP, 36(12), pp. 1846 - 1853, 1988.

[17] V. S. Levine, Ed., *The Control Handbook*, CRC Press and IEEE Press, 1996.

[18] G. J. Tortora and S. R. Grabowski, Principles of Anatomy and Physiology, 8th Edition, HarperCollins Publishers, Inc., Menlo Park, CA, 1996.

[19] http://www.tpub.com/corpsman/14295_files/image074.jpg

[20] http://www.marfan.org/pub/resourcebook/ heartandblood.html

[21] http://www.yoursurgery.com/ProcedureDetails.cfm?BR=5&Proc=68

[22] A. C. Guyton and J. E. Hall, *Textbook of Medical Physiology*, 9th Edition, W. B. Saunders Company, Philadelphia, PA, 1996.

[23] R. M. Berne and M. N. Levy, *Physiology*, 4th Edition, Mosby, Inc., St. Louis, Missouri, 1998.

[24] M. F. O'Rourke and T. Yaginuma, "Wave reflections and the arterial pulse," *Archives of Internal Medicine*, 144(2), pp. 366 - 371, 1984.

[25] Welkowitz, W., *Engineering Hemodynamics: Application to Cardiac Assist Devices*, 2nd Edition, New York University Press, New York, 1987.

[26] E. T. Ozawa, "*A numerical model of the cardiovascular system for clinical assessment of the hemodynamic state*," MIT Ph.D. Thesis, Department of Mechanical Engineering, MIT, September 1996.

[27] E. T. Ozawa, *et al.*, "Numerical simulation of enhanced external counterpulsation," *Annals of Biomedical Engineering*, 29(4), pp.284 - 297, 2001.

[28] N. Stergiopulos, *et al.*, "Evaluation of methods for estimation of total arterial compliance," *American Journal of Physiology, Heart Circulation Physiology*, 268(37), pp. H1540 - H1548, 1995.

[29] R. Mukkamala and R. J. Cohen, "*A forward model-based validation of cardiovascular system identification*," *American Journal of Physiology, Heart Circulation Physiology*, 281, pp. H2714 - H2730, 2001.

[30] R. Mukkamala, "*A Forward Model-based Analysis of Cardiovascular System Identification Methods*," MIT Ph.D. Thesis, Department of Electrical Engineering and Computer Science, MIT, June 2000.

[31] M. F. O'Rourke, *Arterial Function in Health and Disease*, Churchill Livingstone, New York, 1982.